REPORT DOCUMENTATION PAGE

Form Approved
OMB No. 0704-0188

1. AGENCY USE ONLY (Leave blank)	2. REPORT DATE	3. REPORT TYPE AND DATES COVERED
	3/6/97	Annual Technical Report 4/96-3/97

4. TITLE AND SUBTITLE
Metalorganic Chemical Vapor Deposition of GaN, AlN, and GaAlN for UV Photodetector Applications

5. FUNDING NUMBERS
N00014-93-1-0235

6. AUTHOR(S)
M. Razeghi

7. PERFORMING ORGANIZATION NAME(S) AND ADDRESS(ES)
Northwestern University
Center for Quantum Devices
2225 N. Campus Drive, MLSB Room 4051
Evanston, IL 60208-3118

8. PERFORMING ORGANIZATION REPORT NUMBER

9. SPONSORING / MONITORING AGENCY NAME(S) AND ADDRESS(ES)
Office of Naval Research
800 N. Quincy Street
Arlington, VA 22217-5660

BMDO
7100 Defense;Pentagon
Washington, DC
20301-7100

10. SPONSORING / MONITORING AGENCY REPORT NUMBER

11. SUPPLEMENTARY NOTES

12a. DISTRIBUTION / AVAILABILITY STATEMENT
Approved for Public Release; Distribution Unlimited

13. ABSTRACT *(Maximum 200 words)*

The cause of the X-ray diffraction peak broadening in GaN epilayers grown on sapphire (Al_2O_3) substrates was investigated and attributed to a limited in-plane coherence length. Screw and mixed dislocation densities less than ~10^7 cm^{-2} were achieved in GaN epilayers on Al_2O_3. On the same Al_2O_3 wafer, up to two inches in diameter, GaN films exhibited mirror-like surface morphologies, good uniformity, narrow X-ray diffraction (30 arcsecs) and narrow bandedge photoluminescence emission lines (17 meV at 77K). The n-type and p-type doping control of GaN were improved (n up to ~10^{20} cm^{-3} and μ_n increased to >300 cm^2/Vs, while p increased up to $3x10^{17}$ cm^{-3} at 300K). The quality of $Al_xGa_{1-x}N$ films on Al_2O_3 ($0 \le x \le 1$) was improved. The (00•2) X-ray diffraction linewidths were <4 arcmins. The n-type and p-type doping control of $Al_xGa_{1-x}N$ were achieved up to Al concentrations of 50% and 30%, respectively. $Al_xGa_{1-x}N$-based Bragg reflectors, two dimensional electron gas structures, $Al_xGa_{1-x}N$/GaN superlattices exhibiting clear X-ray diffraction satellite peaks (up to the 10th peak) were demonstrated. The atomic sharpness of the interfaces was confirmed through cross-sectional transmission electron microscopy. Monocrystalline GaN was grown on quasi lattice-matched β-$LiGaO_2$ substrates by MOCVD, with X-ray diffraction linewidths of 300 arcsecs and intense near bandedge photoluminescence. $Al_xGa_{1-x}N$-based ultraviolet photoconductors were achieved with cut-off wavelengths from 365 to 200 nm. Detectivities D* were measured to be ~10^9 cm·$Hz^{1/2}$/W. After the dry etching system was installed, GaN p-i-n mesa structures were fabricated. ***The response speed of these photodiodes was significantly increased and was limited by the circuit RC time constant.***

14. SUBJECT TERMS
X-ray, GaN, n-type, p-type, $Al_xGa_{1-x}N$, Al concentration, two dimensional electron gas, Bragg reflectors, superlattices, satellite peaks, atomic sharpness, transmission electron microscopy, ultraviolet, lattice-matched, β-$LiGaO_2$, photoconductors, cut-off wavelength, D*, dry etching, mesa, photodiode, response speed

15. NUMBER OF PAGES
70

16. PRICE CODE

17. SECURITY CLASSIFICATION OF REPORT	18. SECURITY CLASSIFICATION OF THIS PAGE	19. SECURITY CLASSIFICATION OF ABSTRACT	20. LIMITATION OF ABSTRACT
Unclassified	Unclassified	Unclassified	

Metalorganic Chemical Vapor Deposition of GaN, AlN, and GaAlN for UV Photodetector Applications

BMDO/ONR Contract #N00014-93-1-0235

Program Managers: Max Yoder, ONR
Colin Wood, ONR

Development of III-Nitride Technology for Optoelectronic Devices

DARPA/ONR Contract #N00014-96-1-0714

Program Managers: Anis Husain, DARPA
Yoon-Soo Park, ONR

Annual Technical Report 4/96 - 3/97

Principal Investigator: Manijeh Razeghi

Center for Quantum Devices
Department of Electrical and Computer Engineering
Northwestern University, Evanston, IL 60208
Tel: (847) 491-7251
Fax: (847) 467-1817
E-mail: razeghi@ece.nwu.edu

Staff: Jianren Xu

Students: Patrick Kung
Adam Saxler
Xiaolong Zhang
Rosario Lavado
Danielle Walker

ABSTRACT

The research work on III-Nitride semiconductors (AlN, GaN and $Al_xGa_{1-x}N$) conducted at Center for quantum Devices (CQD) at Northwestern University during the past year will be presented in this report. Our previous work has been described in earlier reports.

In order to understand the nature of structural defects in GaN thin films on sapphire substrates, CQD has investigated the cause of the X-ray diffraction peak broadening in GaN epilayers grown on sapphire substrates. We have studied the reciprocal space maps of symmetric and asymmetric GaN X-ray reflections and shown that the primary cause was a limited in-plane coherence length, which is consistent with transmission electron microcopy analysis.

We have demonstrated the reduction of the density of screw and mixed **dislocation densities** in GaN epilayers on sapphire substrates to **less than ~10^7 cm^{-2}**, as measured by cross-sectional transmission electron microscopy. The structure employed involved alternating layes of GaN and $Al_xGa_{1-x}N$. The micrograph showed how the dislocations were annihilated at each successive interface, leaving only less than 10^7 cm^{-2} in the top GaN layer.

In an on-going effort to improve the III-Nitride material quality, CQD has been developing the metalorganic chemical vapor deposition (MOCVD) of III-Nitrides. By further optimizing the growth conditions, we have achieved GaN thin films on sapphire substrates with mirror-like surface morphologies, good uniformity, narrow X-ray diffraction (30 arcsecs) and narrow bandedge photoluminescence emission lines (17 meV at 77K) **on the same wafer, with wafer sizes up to two inches in diameter.** The n-type doping control of GaN using both silicon and germanium has been achieved up to n(300K)~10^{20} cm^{-3} and **electron mobilities have been increased to higher than 300 cm^2/Vs** at 300K. The p-type doping control has been improved and **hole concentrations have been increased to 3x10^{17} cm^{-3}** at 300K.

CQD has **improved the quality of its $Al_xGa_{1-x}N$ thin films** on sapphire substrates for the entire composition range from GaN (x=0) to AlN (x=1) by reducing the linewidths of the (00•2) X-ray diffraction peaks to **lower than 4 arcmins**, which confirms the excellent structural quality of the films. The **n-type doping of $Al_xGa_{1-x}N$** up to an **Al concentration of 50%** has been achieved by using SiH_4. Electron mobilities were higher than 80 cm^2/Vs. The p-type doping of $Al_xGa_{1-x}N$ was achieved by using Mg from GaN up to an Al concentration of 30%, We have

successfully demonstrated **$Al_xGa_{1-x}N$-based Bragg reflectors** with controlled peak reflectivity wavelengths, **two dimensional electron gas (2DEG)** structures, $Al_xGa_{1-x}N$/GaN heterostructures and superlattices exhibiting **clear satellite peaks in the X-ray diffraction spectra (up to the 10th peak)**. These confirm the quality of the interfaces in these structures, which is consistent with the atomic sharpness observed by cross-sectional transmission electron microscopy.

In an on-going effort to investigate novel substrate materials for the MOCVD growth of GaN, CQD has investigated the potential of lithium metagallate (β-$LiGaO_2$). **Single crystalline GaN thin films on $LiGaO_2$ substrates have been grown by MOCVD**. The X-ray diffraction linewidths were about 300 arcsecs and the samples exhibited near bandedge photoluminescence at room temperature. This confirms the potential of this new substrate material which is quasi-lattice matched to GaN.

CQD has made **significant advances in the development of ultraviolet photodetectors**. Photoconductors with tailored cut-off wavelengths from 365 to 200 nm have been achieved, by controlling the alloy composition from GaN to AlN. **Detectivity measurements have been performed** and a D* of ~10^9 cm·$Hz^{1/2}$/W was measured at 14 Hz for GaN.

Finally, in the area of material processing, we have conducted a survey of the state-of-the-art of dry etching of III-V nitrides reported in the literature in order to develop our etching capabilities as quickly as possible. Once the PlasmaTherm 770 Dry Etching System was installed, GaN p-i-n mesa structures were fabricated. **The response speed of these p-i-n photodiodes was significantly increased** in comparison to our previous work and **is now limited by the electrical circuit RC time constant.**

Table of contents

I. HIGH RESOLUTION X-RAY DIFFRACTION OF GaN GROWN ON SAPPHIRE SUBSTRATES

I.1. Introduction

GaN based material is ideal for the fabrication of short wavelength optoelectronic devices. The wide direct bandgap of GaN (3.4 eV) combined with its strong bond strength make it an excellent candidate for short wavelength lasers. A major problem with the growth of GaN has been the absence of a high quality lattice matched substrate. Most GaN growth has been performed on basal plane sapphire substrates resulting in films with many defects in the crystal lattice. Nucleation layers of AlN or low temperature GaN are used to promote quasi-two dimensional growth, dramatically improving the properties of the GaN epilayers [1].

The full width at half maximum (FWHM) of the x-ray rocking curve is often used to assess the crystalline quality of GaN epilayers because of the relatively simple nature of this technique. A full understanding of the rocking curves is needed if they are to be used as a reliable indicator of epitaxial quality. In order to understand the information given by the line shape, we need to know the primary mechanism by which the curves are broadened.

Recently, very narrow x-ray rocking curves of epitaxial GaN grown on (00•1) sapphire with a FWHM of under 40 arcsecs have been obtained by several researchers [2-5]. A better understanding of the defects in GaN has recently been established through x-ray diffraction and transmission electron microscopy (TEM) studies [5,6]. The primary defects are threading dislocations running along the c axis, with the majority being edge type with a Burger's vector of 1/3<11•0> although screw and mixed type dislocations have also been seen. In highly dislocated materials, low angle grain boundaries form. In this section, we report the analysis of symmetrical and asymmetrical reciprocal space maps to determine what types of imperfections are responsible for the broadening of x-ray rocking curves in GaN.

I.2. Experimental

The GaN samples used in this study were grown on sapphire substrates with a thin AlN buffer by low pressure MOCVD. The sources used were ammonia, trimethylgallium, and trimethylaluminum in a hydrogen carrier gas. The growth conditions for similar samples were discussed in more detail previously [2]. Samples with a wide range of growth conditions were chosen to establish the generality of the type of broadening of x-ray rocking curves in GaN. The

growth conditions are presented in Table I. GaN films with both broad and very narrow (open detector linewidth of 40 arcsecs for the (00•2) GaN reflection) rocking curves are examined in this work.

The x-ray diffraction experiments were performed using a Philips (MRD) high-resolution triple axis diffractometer [7,8]. TEM samples were examined using a Hitachi HF-2000 with a field emission gun operated at 200 keV.

Sample ID	Sapphire substrate orientation	Buffer layer: thickness (nm), growth T (°C)	Growth pressure (mbar)	Thickness (μm)	Growth T (°C)
A (201)	(00.1)	AlN, 16, 850 C	100	1.2	1000
B (114)	(00.1)	AlN, 34, 1000 C	10	1.1	1000
C (23)	(01.2)	GaN, 23, 600 C	10	1.1	1000

Table I. Growth conditions for the GaN films used in this study.

I.3. Results and discussion

In order to determine the nature of the x-ray broadening in epitaxial GaN, several reciprocal lattice points were mapped. Figure 1(a) shows a reciprocal space map of the (00•2) GaN peak. The most significant broadening is in the w direction, but from this symmetric peak, we cannot distinguish between broadening due to random tilt or curvature and a finite in-plane coherence length. Pendellösung fringes are clearly visible in the $\omega/2\theta$ direction due to the finite thickness and high structural quality of the epilayer. The spacing corresponds to a thickness of 1.2 μm, in good agreement with the thickness measured by ball polishing and optical transmission interference fringes.

A conventional rocking curve of the (00•2) GaN peak yielded a FWHM of 40 arcsecs as illustrated in Figure 1(b). For comparison, the normalized cross sections of the reciprocal space map are also shown in Figure 1(b). (The ω curve and the $\omega/2\theta$ curve are the traces through the peak in Figure 1(a) along the ω and $\omega/2\theta$ directions respectively.) The ω curve has a FWHM of 29 arcsecs, while the $\omega/2\theta$ curve has a FWHM of 16 arcsecs. The ω curve makes the dominant contribution to the broadening of the conventional rocking curve, especially in its broad tails, which obscure the fringes. From this information, we can determine that the broadening is primarily due

to either a limited coherence length parallel to the film surface or from random tilt or curvature of the film.

Investigation of a reciprocal space map of an asymmetrical peak can indicate if the broadening is due to random tilt or curvature or if it is due to a limited in plane coherence length. The (11•4) GaN peak of Sample A is shown in Figure 2. The (11•4) planes are approximately 39 degrees from the (00•1) planes, allowing the different types of broadening to be easily distinguished. From Figure 2(a), the peak is clearly not oriented along ω, which would be expected if curvature or random tilt caused the broadening. When the same peak is plotted in reciprocal space in Figure 2(b), the broadening is nearly entirely along X, indicative of a limited in-plane coherence length. A small tilt from the horizontal may be due to a contribution of broadening in ω. Two peaks on opposite sides of the origin in reciprocal space were used to determine whether the small tilt from the horizontal is due to broadening in ω or due to the discontinuities not being normal to the surface. The tilts are in opposite directions (Figure 3), consistent with a small contribution of ω broadening. A separate measurement of the peak position as a function of the wafer position indicated a small curvature of 20 m, which contributes to the ω broadening in addition to any random tilts.

The TEM results show that edge threading dislocations dominate with a density of approximately 5×10^9 cm^{-2}. In a plan view image with a **g** vector of 11•0 the dislocations appear to be randomly distributed rather than aligned to form low angle grain boundaries. Both edge and screw dislocations are present in the sample as seen by cross sectional images taken using different **g** vectors. The role of these dislocations in the x-ray line broadening is to disrupt the in-plane coherence length in the GaN film.

The rocking curve linewidth was much broader for the second sample of GaN grown on (00.1) sapphire, however, the primary cause for broadening was the same. The symmetrical reciprocal space map is shown in Figure 4(a) and traces through the map are plotted along with the open detector rocking curve in Figure 4(b). Only a small fraction of the broadening is in the ω/2θ direction. Figure 4(c) shows an asymmetrical reciprocal lattice point which is oriented along X in reciprocal space, again indicating a limited in-plane coherence length.

The GaN grown on a (01•2) sapphire substrate was also studied. Figures 5(a) and 5(b) show the symmetrical reciprocal lattice point which again is primarily broadened along ω. The asymmetrical reciprocal lattice point is shown in Figure 5(c). The alignment along X is once again indicative of a limited in-plane coherence length.

The full widths at half maxima for the samples are shown in Table II. The primary broadening for all of the samples studied is along X, rather than Y, ω, or ω/2θ. This is indicative of a limited in-plane coherence length. The in-plane coherence length can be estimated by a simple equation for symmetric reflections: $d = 0.89 \lambda / 2 \Delta\omega \sin\theta, \lambda$ where is the x-ray wavelength, $\Delta\omega$ is the FWHM of the rocking curve, and θ is the Bragg angle. However, for randomly sized domains, the coherence length obtained will reflect the longer coherence lengths present in the sample. This type of broadening is consistent with the wide tails commonly present in rocking curves of GaN.

GaN peak	ω (arcsec)	ω/2θ (arcsec)	X (A^{-1} x 10^{-4})	Y (A^{-1} x 10^{-4})
Sample A (201)				
(00•2)	29	16	0.539	0.973
(00•4)	56	21	2.02	1.05
(00•6)	62	51	3.5	1.5
(11•4)	72	56	7.1	2.1
(20•4)	50	58	9.5	2.2
($\bar{2}$0•4)	64	76	10	3.0
Sample B (114)				
(00•2)	667	32	12.5	1.8
(00•4)	684	41	25.5	2.1
(11•4)	220	140	10	5
(10•4)	220	130	20	4
Sample C (23)				
(11•0)	1620	61	49	3.6
(11•2)	430	110	47	8.4
(02•0)	360	270	50	7.5

Table II. FWHM of various GaN reflections.

I.4. Conclusions

In summary, reciprocal space mapping of both symmetric and asymmetric reflections was used to determine the primary cause for broadening of the epitaxial GaN x-ray rocking curves.

The broadening was shown to be due to a limited in-plane coherence length. This is consistent with TEM studies that show threading dislocations originating at the interface, presumably during the initial stages of growth and island coalescence. These dislocations disrupt the coherence length, resulting in broadening of the x-ray rocking curve.

I.5. References

[1]. K. Hiramatsu, S. Itoh, H. Amano, I. Akasaki, N. Kuwano, T. Shiraishi, and K. Oki, J. Cryst. Growth **115**, 628 (1991).

[2]. P. Kung, A. Saxler, X. Zhang, D. Walker, T. C. Wang, I. Ferguson, and M. Razeghi, Appl. Phys. Lett. **66**, 2958 (1995).

[3]. K. G. Fertitta, A. L. Holmes, J. G. Neff, F. J. Ciuba, and R. D. Dupuis, Appl. Phys. Lett. **65**, 1823 (1994).

[4]. W. E. Plano, J. S. Major, Jr., D. F. Welch and J. Speirs, Electron. Lett. **30**, 2079 (1994).

[5]. B. Heying, X. H. Wu, S. Keller, Y. Li, D. Kapolnek, B. P. Keller, S. P. DenBaars, and J. S. Speck, Appl. Phys. Lett. **68**, 643 (1996).

[6]. W. Qian, M. Skowronski, M. De Graef, K. Doverspike, L. B. Rowland, and D. K. Gaskill, Appl. Phys. Lett. **66**, 1252 (1995).

[7]. P. F. Fewster, J. Appl. Cryst. **22**, 64 (1989).

[8]. P. F. Fewster, Appl. Phys. A **58**, 121 (1994).

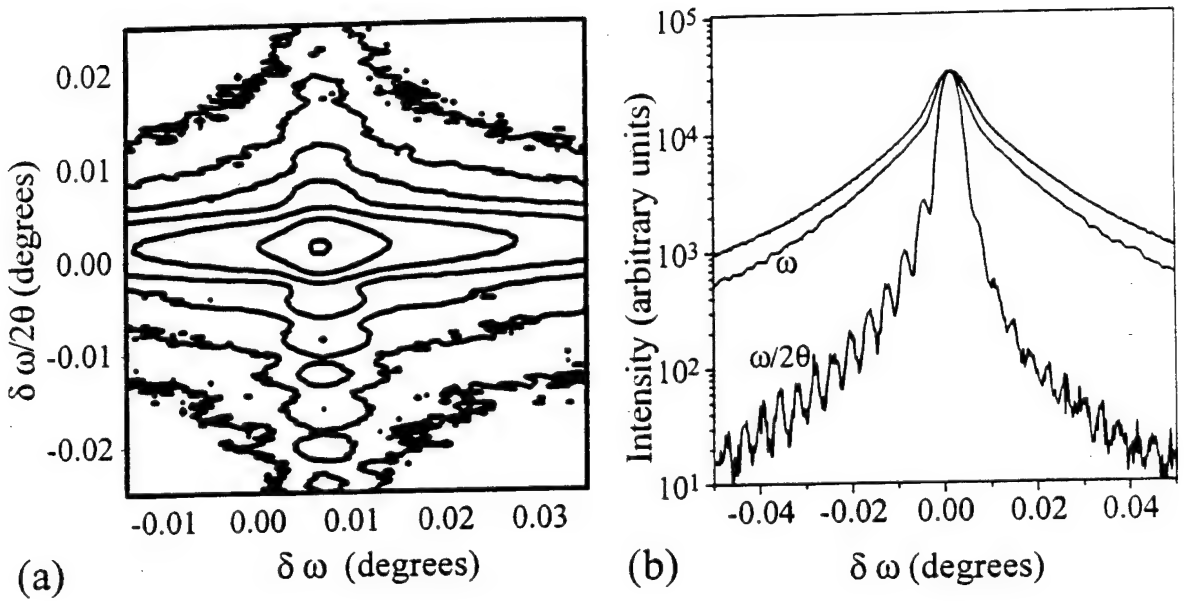

Figure 1. (a) Reciprocal space map of the (00•2) GaN peak of Sample A. Interference fringes due to the finite film thickness are clearly visible in the ω/2θ direction. Isointensity contours are logarithmically spaced by a factor of $10^{0.5}$. (b) Open detector rocking curve, triple axis ω scan, and triple axis ω/2θ scan of the (00•2) GaN peak of Sample A.

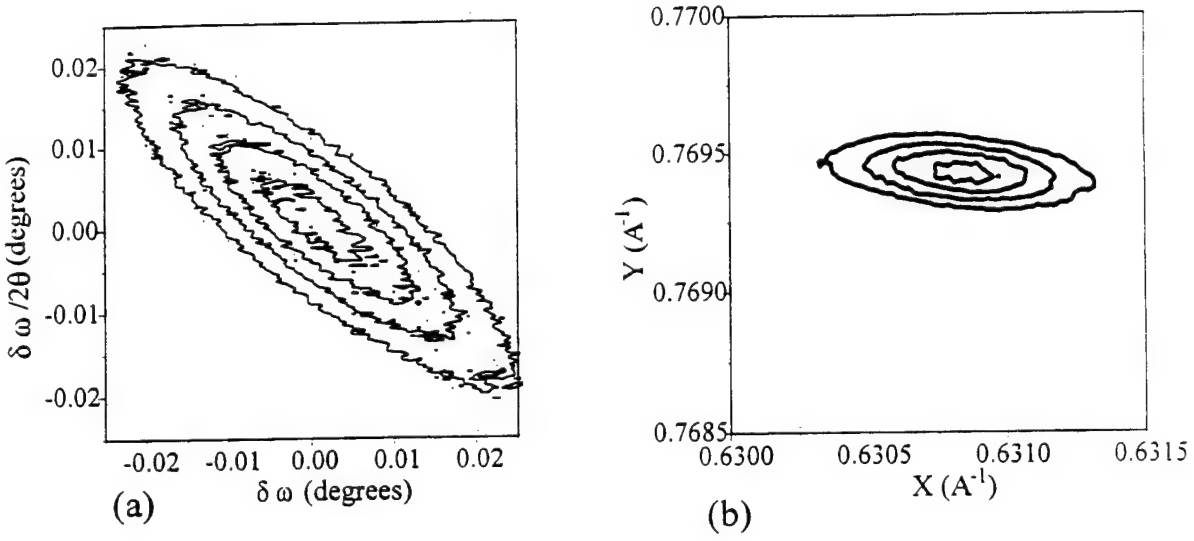

Figure 2. Reciprocal space map of the (11•4) GaN peak of Sample A plotted in degrees (a) and reciprocal lattice units (b). This shows that the primary cause of broadening is due to a limited in-plane coherence length rather than tilt or curvature.

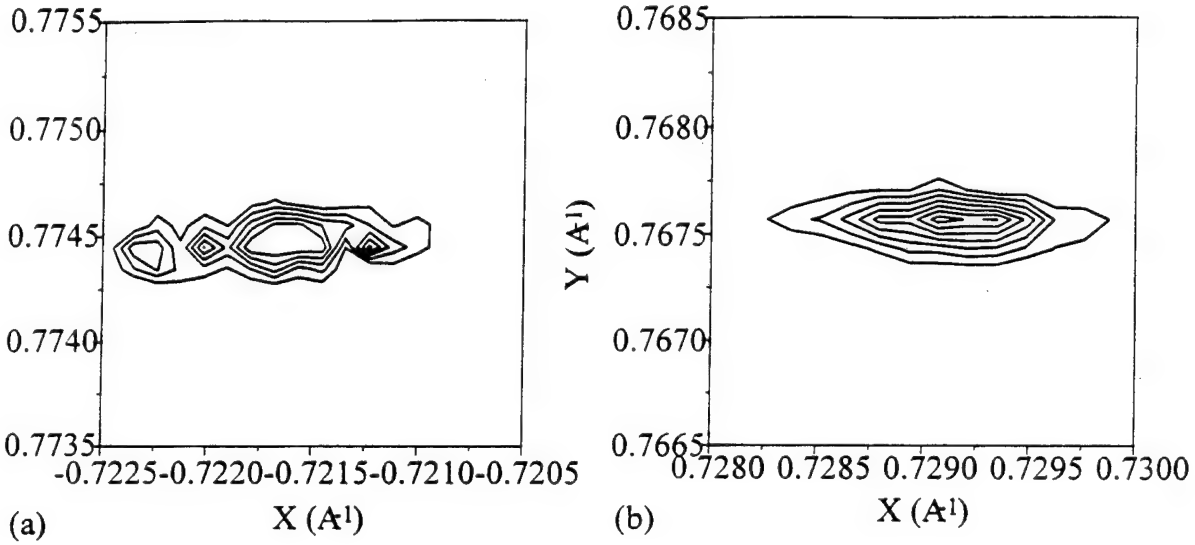

Figure 3. Reciprocal space maps of the (a) (-20•4) and (b) (20•4) GaN peaks of Sample A showing that there is a small curvature or tilt component rather than dislocations slightly off normal to the surface.

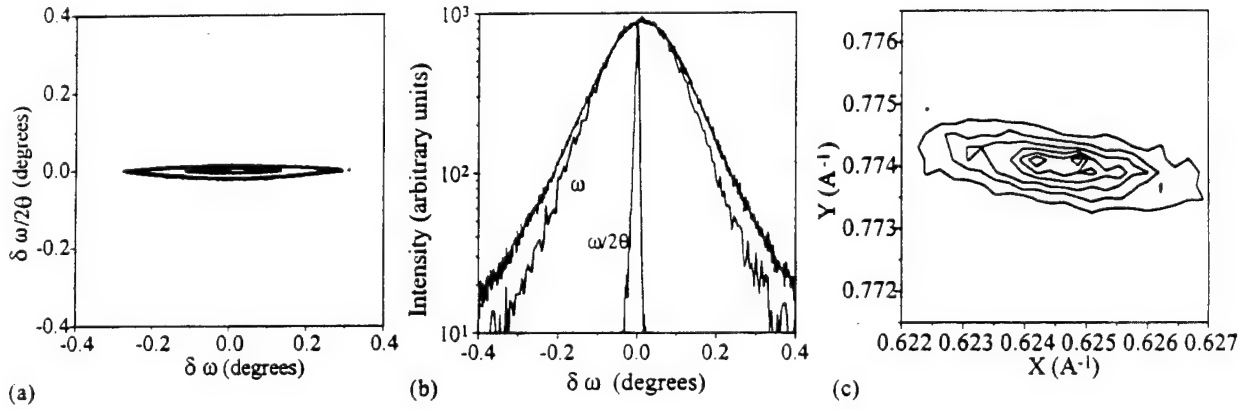

Figure 4. (a) Symmetrical reciprocal space map of the (00•2) GaN peak of Sample B. (b) Open detector rocking curve, triple axis ω scan, and triple axis ω/2θ scan of the (00•2) GaN peak of Sample B. (c) Asymmetrical reciprocal space map of the (11•4) GaN peak of Sample B.

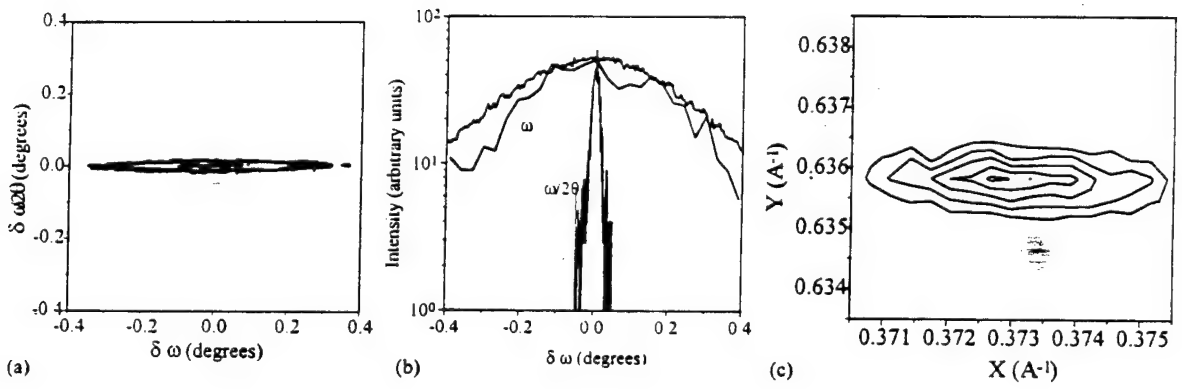

Figure 5. (a) Symmetrical reciprocal space map of the (11•0) GaN peak of Sample C. (b) Open detector rocking curve, triple axis ω scan, and triple axis ω/2θ scan of the (11•0) GaN peak of Sample C. (c) Asymmetrical reciprocal space map of the (11•2) GaN peak of Sample C.

II. MICROSTRUCTURAL CHARACTERIZATION OF GaN THIN FILMS ON SAPPHIRE SUBSTRATES

II.1. Introduction

Wide bandgap III-Nitrides (AlN, GaN, InN and alloys thereof) are superior to other semiconductor materials for photonic devices operating in the visible-ultraviolet (UV) spectral range. These materials cover a large spectral bandwidth (650 to 200 nm), and large heterojunction band offsets can be achieved. They are physically hard, strong against radiations, thermally stable, they have high thermal conductivities, high charge carrier velocities and low dielectric constants. These properties are expected to extend the reliability and lifetime of devices made from III-Nitride materials.

Photonic devices such as blue/UV light emitting and laser diodes, solar-blind UV photodetectors find their applications in high brightness flat panel displays, high density optical storage, underwater communications, space-to-space communications secure from earth and missile detection above the ozone layer where there is a strong visible and infrared background.[1,2]

For the past decade, most of the research effort has focused on the synthesis of device quality materials. It is only recently that high quality photonic devices, such as blue/UV light emitting diodes (LED's) [3], laser diodes [4] and UV photodetectors [5-7] have been demonstrated. However, the material used in these devices is still defective. For instance, the density of threading dislocations in the GaN-based blue/UV LED's is typically ~10^{10} cm^{-2}.[8] This number is very large, considering that dislocation densities of ~10^{4} cm^{-2} can limit the efficiencies of GaAs based LED's. To improve the reliability and lifetime of GaN-based devices, in particular blue/UV laser diodes and solar-blind UV photodetectors, the dislocation densities need to be reduced below 10^{5} cm^{-2} in GaN-based materials.

The present work reports a methodology to reduce the density of screw and mixed dislocations, below 10^{7} cm^{-2}, in GaN/AlGaN heterostructures grown the metalorganic chemical vapor deposition (MOCVD).

II.2. Experimental

The AlN, GaN and $Al_xGa_{1-x}N$ thin films were deposited on basal plane sapphire substrates, (00•1) α-Al_2O_3. The substrates were placed on a SiC-coated graphite susceptor, into a horizontal low-pressure MOCVD reactor (AIXTRON 200/4 SiC). The susceptor was RF-heated and spun at a speed of ~60 rpm to increase the epilayer uniformity across the wafers. The growth pressure ranged from 10 to 100 mbar. The source materials include trimethyl-aluminum, trimethyl-gallium, triethyl-gallium and ammonia. The carrier gases were hydrogen and purified nitrogen. The Al and Ga molar flow rates ranged from 10 to 40 µmol/min, while the V/III ratio was between 1000 and 3000.

The AlN films were deposited directly on (00•1) α-Al_2O_3 substrates at a growth temperature ~1000 °C, with a growth rate of ~0.15 µm/hr. For the growth of GaN films, we first deposited a thin (~350 Å) AlN buffer layer [9] using the same growth conditions as described previously. The growth temperature for GaN was also ~1000 °C and the growth rate was ~0.7 µm/hr. The growth conditions for the $Al_xGa_{1-x}N$ films were similar to those of GaN and the composition was controlled by varying the Al to Ga molar ratio.

High resolution X-ray diffraction measurements and transmission electron microscopy (TEM) were conducted to assess the structural and microstructural properties of the films. The TEM specimens were realized by first M-bonding two pieces face-to-face. They were then mechanically polished down to a thickness of ~10 µm, followed by Ar^+ ion milling (5 kV, 0.5 mA) to reach electron transparency. TEM observations were carried out on a Hitachi HF 2000 field-emission microscope operated at 200 keV. The absorption edge of the $Al_xGa_{1-x}N$ compounds for $0 \leq x \leq 1$ was determined through optical absorption.

II.3. TEM of a GaN/AlGaN/GaN heterostructure

Upon optimizing $Al_xGa_{1-x}N$ thin films for $0 \leq x \leq 1$, we grew a GaN/AlGaN double heterostructure which consisted of a 0.7 µm $Al_{0.33}Ga_{0.67}N$ layer sandwiched between two 0.6 µm GaN layers. The structure was grown on (00•1) Al_2O_3 using a thin (~350 Å) AlN buffer layer. The sequence of layers in this structure was selected in order to help the relaxation of stress due to lattice mismatch, as will be discussed later.

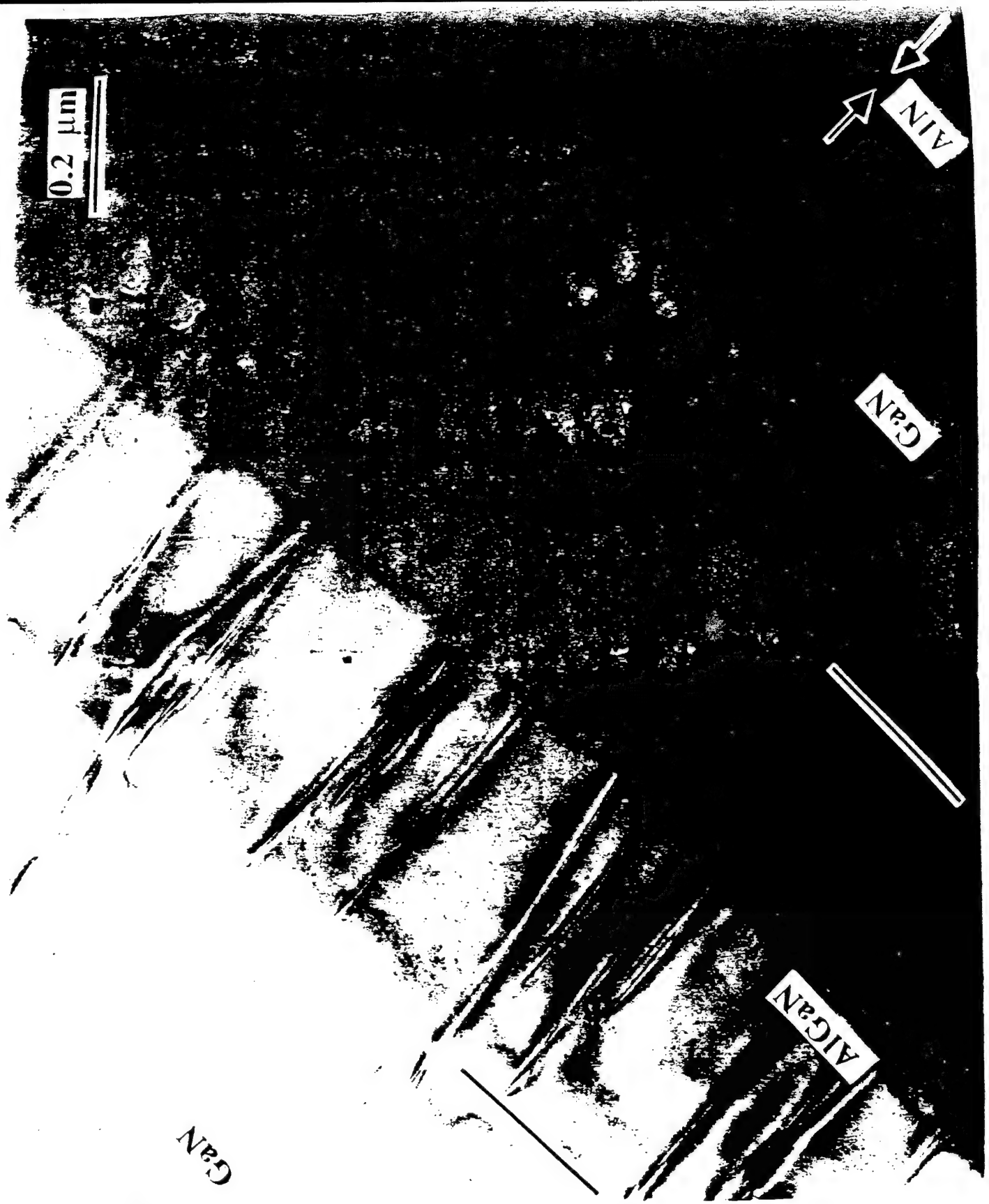

Figure 1. Cross sectional bright field TEM micrograph of a GaN / $Al_{0.33}Ga_{0.67}N$ / GaN heterostructure grown on (00•1) Al_2O_3.

Figure 1 shows the cross sectional bright field TEM micrograph of this heterostructure with **g**=00•2. The threading dislocations that can be seen are screw dislocations or have a mixed character, which have Burgers vectors non perpendicular to **g**. The bottom GaN layer, closer to the sapphire substrate, is highly defective. The high density of dislocations does not seem to be reduced with the thickness of the GaN film up to 0.6 μm. By contrast, in the $Al_{0.33}Ga_{0.67}N$ layer, it is significantly reduced. More importantly, Figure 1 shows how the screw and mixed dislocations visible in this configuration are stopped at each successive interface. It shows how the screw and mixed dislocation density can be reduced. In the top GaN layer, an estimate of the dislocations yields $< \sim 10^7$ cm^{-2}, which is the density of the screw and mixed dislocations that threaded through the second GaN/AlGaN interface.

A simple interpretation for the annihilation of dislocations at each interface is the way the stress due to the lattice mismatch is relaxed through the heterostructure. GaN has a large (~16 %) lattice mismatch with (00•1) Al_2O_3, which results in a significant amount of compressive stress at the interface between GaN and the sapphire substrates, as well as a large amount of misfit dislocations in the interface plane.[10] By using an AlN buffer layer, the stress in GaN is somewhat reduced because there is only a ~2.5 % lattice mismatch between GaN and AlN, but the GaN film will still be under compressive stress because its lattice constant in the *c*-plane (3.189 Å) is larger than that of AlN (3.112 Å) in the same plane. By using layers with graded lattice parameters (e.g. $Al_xGa_{1-x}N$) from AlN to GaN, the lattice mismatch can be gradually reduced. But the stresses due to the lattice mismatch would remain compressive at all the interfaces.

In the case of our structure, by sandwiching a $Al_{0.33}Ga_{0.67}N$ layer between two GaN layers, the stress is reversed: it is first compressive (for GaN on the AlN buffer) and becomes tensile (for $Al_{0.33}Ga_{0.67}N$ on GaN). It is then compressive again (for GaN on $Al_{0.33}Ga_{0.67}N$). By inverting the stress at successive interfaces, the screw and mixed dislocations bend and are stopped by annihilating themselves with the misfit dislocations formed at teach interfaces, as shown in Figure 1.

II.4. TEM of a GaN/AlGaN superlattice

It is well known that multilayers are effective in reducing the density of threading dislocations in conventional III-V compounds.[11] In order to further reduce the dislocation density in GaN, we grew a structure which consisted of a 15 period {50Å-GaN / 100Å-$Al_{0.33}Ga_{0.67}N$} superlattice (SL), sandwiched between two 0.1 μm thick $Al_{0.33}Ga_{0.67}N$ layer, on a

0.8 μm thick GaN. This structure is similar to the one previously discussed by replacing the top GaN layer with the superlattice.

Figure 2 shows the cross sectional bright field TEM micrograph of this superlattice structure with **g**=00•2. The same types of screw and mixed threading dislocations can be seen. The propagation of these dislocations does not seem to be stopped at the GaN/AlGaN interfaces in the superlattice but rather goes through the entire SL structure. This can be explained by the fact that the thicknesses of each layer in the SL are too small to modify the stress profile across the structure.

Figure 2 also shows the excellent sharpness control of the GaN/AlGaN interfaces. We were able to confirm the expected period layer thicknesses in the superlattice. A high resolution bright field TEM micrograph of the SL structure is shown in Figure 3, demonstrating the interfaces are atomically smooth. The X-ray diffraction spectrum of such superlattices will be discussed in Section IV.

II.5. Conclusions

We have reported the MOCVD growth and characterization of high quality AlN, GaN and $Al_xGa_{1-x}N$ thin films on Al_2O_3 substrates. By sandwiching a AlGaN layer between two GaN layers, we have reduced the density of screw and mixed dislocations in GaN to less than ~10^7 cm^{-2}. Atomically sharp interfaces in 50Å-GaN / 100Å-AlGaN superlattice structures have been demonstrated by high resolution electron microscopy.

II.6. References and figure captions

[1] R.F. Davis, Physica B **185**, 1 (1993).

[2] M. Razeghi, Y.H. Choi, X. He, and C.J. Sun, Materials Science and Technology **11**, 3 (1995).

[3] S. Nakamura, M. Senoh, N. Iwasa, and S.I. Nagahama, Appl. Phys. Lett. **67** 1868 (1995).

[4] S. Nakamura, M. Senoh, S.I. Nagahama, N. Iwasa, T. Yamada, T. Matsushita, H. Kiyoku and Y. Sugimoto, Jpn. J. Appl. Phys. **35**, L74 (1996).

[5] X. Zhang, P. Kung, D. Walker, J. Piotrowski, A. Rogalski, A. Saxler, and M. Razeghi, Appl. Phys. Lett. **67**, 2028 (1995).

[6] P. Kung, X. Zhang, D. Walker, A. Saxler, J. Piotrowski, , A. Rogalski, and M. Razeghi, Appl. Phys. Lett. **67**, 3792 (1995).

[7] D. Walker, X. Zhang, P. Kung, A. Saxler, S. Javadpour, J. Xu and M. Razeghi, Appl. Phys. Lett. **68**, 2100 (1996).

[8] S.D. Lester, F.A. Ponce, M.G. Craford, and D.A. Steigerwald, Appl. Phys. Lett. **66**, 1249 (1995).

[9] P. Kung, A. Saxler, X. Zhang, D. Walker, T.C. Wang, I. Ferguson, and M. Razeghi, Appl. Phys. Lett. **66**, 2958 (1995).

[10] A. Saxler, P. Kung, C.J. Sun, E. Bigan, and M. Razeghi, Appl. Phys. Lett. **64**, 339 (1994).

[11] J.W. Matthews, and A.E. Blakeslee, J. Cryst. Growth **27**, 118 (1974).

Figure 2. Cross sectional bright field TEM micrograph of a 15 period {50Å-GaN / 100Å-$Al_{0.33}Ga_{0.67}N$} superlattice structure grown on (00•1) Al_2O_3.

Figure 3. High resolution cross sectional bright field micrograph of superlattice structure showing the atomic scale interface sharpness.

III. $Al_xGa_{1-x}N$ BASED MATERIALS, STRUCTURES AND DEVICES

III.1. Introduction

III-Nitride semiconductors, such as AlN, GaN, InN and their alloys, have become the leading material system for wide bandgap, short wavelength, optoelectronics applications because of their exceptional physical properties. III-Nitrides have a direct bandgap which is tunable in energy from 6.2 eV (AlN), 3.4 eV (GaN) to 1.9 eV (InN) making them ideal for high efficiency photonic devices capable of operating from the ultraviolet (UV) to the red spectral regions. Such devices include UV-visible light emitting diodes (LEDs), laser diodes and solar-blind UV photodetectors for high density optical storage, high-brightness color displays, undersea and covert space-to-space communications and the detection of spacecraft above the ozone layer where there is a strong visible and infrared background.

We have already reported the growth and characterization of AlN and GaN epilayers with the narrowest x-ray diffraction linewidths ever reported on sapphire substrates, as measured with an X-ray diffractometer operated in the "open detector mode" [1,2]. The origin of the deep-level associated yellow luminescence in GaN has been attributed to Ga vacancies [3]. High quality metal-insulator-semiconductor devices have been fabricated for the first time using AlN as the insulating layer [4]. GaN p-n homojunction based photovoltaic detectors have been fabricated and modeled [5]. The kinetics of photoconductivity in n-type GaN has been studied [6].

In this paper, we report our progess for GaN thin films on sapphire substrates, followed by the growth and characterization of $Al_xGa_{1-x}N$ thin films on basal plane sapphire substrates in the entire compositional range, the n-type and p-type doping of $Al_xGa_{1-x}N$ as a function of alloy composition and dopant flow rate, the fabrication of Bragg reflectors using $Al_xGa_{1-x}N$ alloys, the observation of a two-dimensional electron gas (2DEG) at $Al_xGa_{1-x}N$/GaN interfaces, the reduction of dislocation densities in $Al_xGa_{1-x}N$/GaN heterostructures and the fabrication of $Al_xGa_{1-x}N$ based ultraviolet photoconductors with cut-off wavelengths from 200 to 365 nm corresponding to the whole range of $Al_xGa_{1-x}N$ alloys.

III.2. Experimental procedures

The thin films were grown using a horizontal low pressure metalorganic chemical vapor deposition reactor (MOCVD). The 4 inch graphite susceptor was RF heated and spun at about

100 rpm to enhance the uniformity of the films. Trimethylaluminum (TMAl), trimethyl- (TMGa) and triethyl-gallium (TEGa) and ammonia (NH_3) were used as the source materials. Dilute silane (35 ppm SiH_4 in H_2) and dilute germane (50 ppm GeH_4 in H_2) were used as the n-type dopant sources, while biscyclopentadienylmagnesium (Cp_2Mg) was used as the p-type dopant source. Organometallic and hydride sources were separated until just before reaching the susceptor to minimize parasitic reactions. The carrier gas was a mixture of hydrogen and nitrogen. The growth temperature was 1000°C and the growth pressure was 10 mbar.

The films were grown on basal plane sapphire (Al_2O_3) substrates. A thin AlN buffer layer was first grown to improve the initial nucleation and enhance two dimensional growth. The growth conditions of the buffer layer are described in detail in a previous report [2].

The structural properties of the films were assessed through various techniques, including X-ray diffraction using a diffractometer operated in the "open detector mode", scanning electron microscopy (SEM) using a Hitachi S4500 field emission microscope and transmission electron microscopy (TEM) using a Hitachi HF2000 field emission microscope. The optical and electrical properties of the films were determined through optical transmission, photoluminescence using a 10 mW He-Cd laser and Hall effect measurements.

III.3. Progress for GaN Thin Films on (00•1) Sapphire

Our previous work on the optimization of the MOCVD growth of GaN thin films has been reported earlier.[2] Since then, the material quality and the n-type and p-type doping of GaN on basal plane sapphire substrates have been further improved.

On the same wafer, GaN thin films exhibited at the same time mirror-like surface morphologies, narrow X-ray diffraction (30 arcsecs) and narrow room temperature and low temperature bandedge photoluminescence emission lines (e.g. 17 meV at 77K). This has also been achieved on wafer sizes up to two inches in diameter with good uniformity.

The n-type doping control of GaN using both silicon and germanium was achieved up to $n(300K) \sim 10^{20}$ cm^{-3} and electron mobilities were increased to higher than 300 cm^2/Vs at room temperature. The p-type doping control was also improved and hole concentrations were increased to 2×10^{17} cm^{-3} at room temperature. Temperature dependent Hall effect measurements were carried out at Wright Laboratory, and the results shown in Figure 1 yielded an activation energy of ~165 meV for the Mg dopant. This value is close to the value measured through temperature dependent photoluminescence.

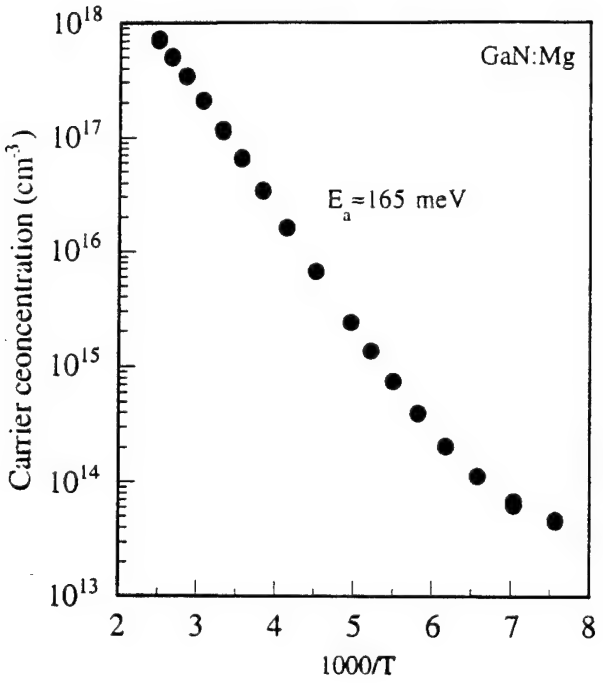

Figure 1. P-type carrier concentration as a function of temperature as measured by temperature dependent Hall effect on a typical GaN:Mg thin film on sapphire substrate.

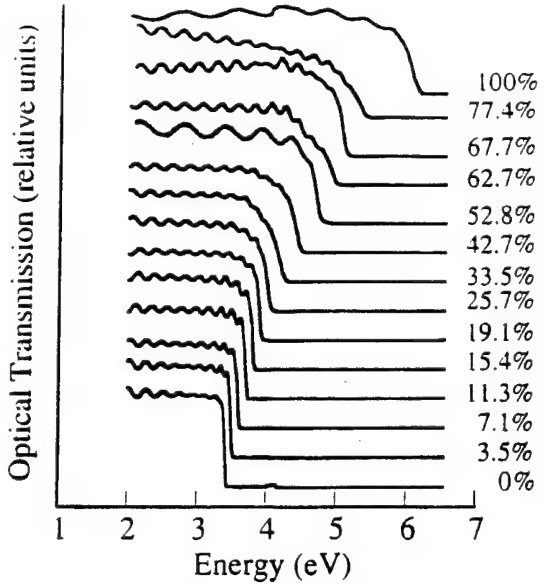

Figure 2. Room temperature optical transmission spectra of $Al_xGa_{1-x}N$ thin films on sapphire substrates.

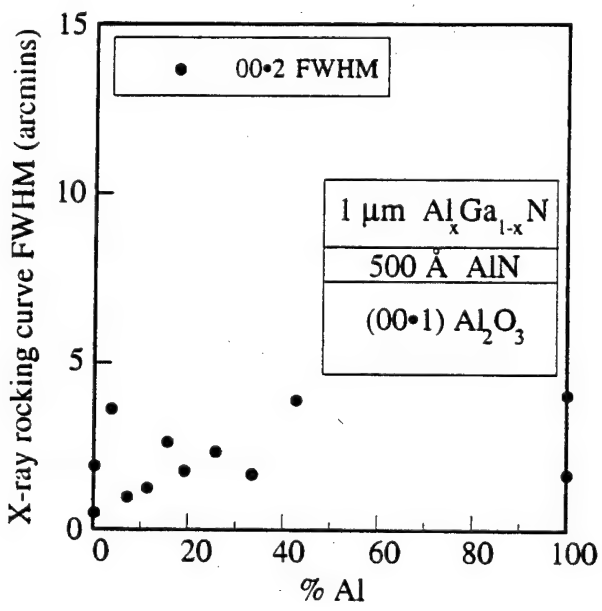

Figure 3. X-ray rocking curve linewidths of selected $Al_xGa_{1-x}N$ thin films on sapphire substrates.

III.4. Undoped $Al_xGa_{1-x}N$ Thin Films on (00•1) Sapphire

The undoped $Al_xGa_{1-x}N$ thin films were grown on sapphire in the same growth conditions as for the GaN epilayers we reported earlier [2], except that the Al source partial pressure in the reactor was varied. The films were about 1 μm thick as determined by SEM, corresponding to a growth rate of about 1 μm/hr. The samples were transparent with smooth surface morphologies, and they were insulating. The alloy composition was determined both by optical transmission and X-ray diffraction. However, the X-ray diffraction peak positions were shifted from their values for bulk films due to significant residual strain in the thin (00•1) $Al_xGa_{1-x}N$ films which resulted from a combination of lattice and thermal mismatch between the film and the Al_2O_3 substrate [7]. Therefore, optical transmission offered a better measure of the Al concentration than X-ray diffraction and this is the method we used in the rest of the paper. Figure 2 shows typical optical transmission spectra of $Al_xGa_{1-x}N$, demonstrating that the entire ternary alloy composition is achieved. Figure 3 shows the X-ray rocking curve linewidths of the 00•2 diffraction peak for selected alloy compositions. The linewidths were lower than 4 arcmins for up to 50% Al, which represents the lowest values ever reported for such $Al_xGa_{1-x}N$ compounds. These linewidths are more than 10 times narrower than those reported in [8].

III.5. Doping of $Al_xGa_{1-x}N$

N-type and p-type doping of $Al_xGa_{1-x}N$ compounds was achieved by incorporating the dopant during the epitaxial growth. Doping was studied as a function of Al concentration and dopant flow rate.

Figure 4 shows the resistivity, electron mobility and concentration in $Al_xGa_{1-x}N$ thin films doped with a fixed flow of SiH_4 as a function of alloy composition. It shows that the resistivity increases exponentially with Al concentration. The values for the resistivity were about 1 order of magnitude lower than those reported in [9] and several orders lower than those reported in [10]. Mobilities as high as 80 cm^2/Vs were measured on $Al_{0.2}Ga_{0.8}N$:Si, which is the highest value ever reported for such a high Al concentration. The graph also shows that $Al_xGa_{1-x}N$ compounds can be n-type doped for an Al concentration higher than 50%, which is very promising for the realization of device structures with large band offsets using III-Nitride materials. This is first time highly conductive $Al_xGa_{1-x}N$ films have been obtained for such high Al concentrations.

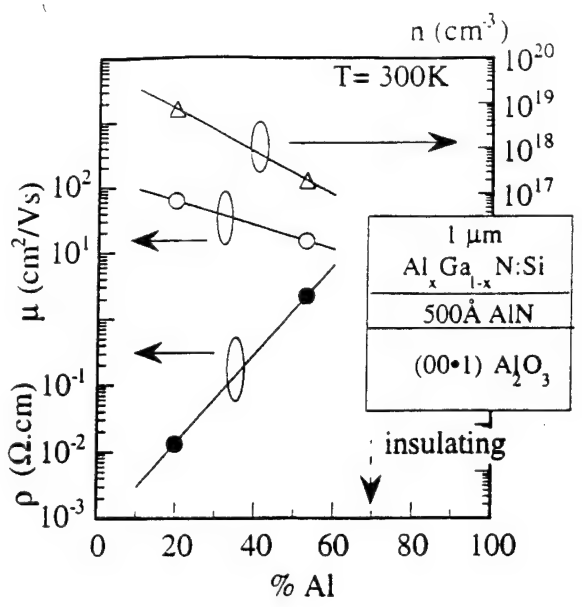

Figure 4. Room temperature resistivity, electron mobility and concentration of Si-doped $Al_xGa_{1-x}N$ thin films.

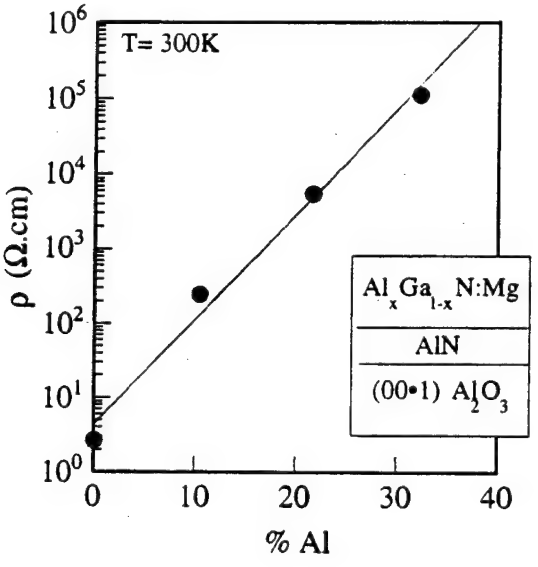

Figure 5. Room temperature resistivity of Mg-doped $Al_xGa_{1-x}N$ thin films.

Figure 5 shows the resistivity of $Al_xGa_{1-x}N$ thin films doped with a fixed flow of Cp_2Mg as a function of alloy composition. In order to activate the incorporated Mg, the samples were subjected to thermal annealing prior to any electrical measurement. Here again, the plot shows that the resistivity increases exponentially with Al concentration, from ~ 2 Ω.cm for GaN up to ~ 10^5 Ω.cm for $Al_{0.3}Ga_{0.7}N$.

The n-type doping of $Al_{0.2}Ga_{0.8}N$ was studied as a function of SiH_4 and GeH_4 flow rates. The carrier concentrations increased linearly with dopant flow rate, up to $3x10^{19}$ cm^{-3}. The surface morphology of the films was not deteriorated by the doping in this range and the films were free from cracks.

III.6. $Al_xGa_{1-x}N$ Based Bragg Reflectors

Building on our success to grow high quality doped $Al_xGa_{1-x}N$ films, we realized Bragg reflectors on basal plane sapphire substrates. They consisted of 20 periods of Si-doped $\{Al_{0.5}Ga_{0.5}N$ / $Al_{0.2}Ga_{0.8}N\}$ multilayers grown on an AlN buffer layer. The period thickness was on the order of 1000 Å, with each layer thickness on the order of 400-500 Å. Figure 6 shows the room temperature optical transmission for selected quarter-wave stacks. The dip in the transmission spectrum corresponds to the peak reflectivity of the structure. A peak reflectivity higher than 60% may be estimated from these curves. By varying the multilayer period thickness, we were able to tune the peak reflectivity from 330 nm to 456 nm. The structures were electrically conductive with high mobilities (~100 cm^2/Vs). These results are very promising for the realization of vertical cavity surface emitting blue lasers using III-Nitride materials.

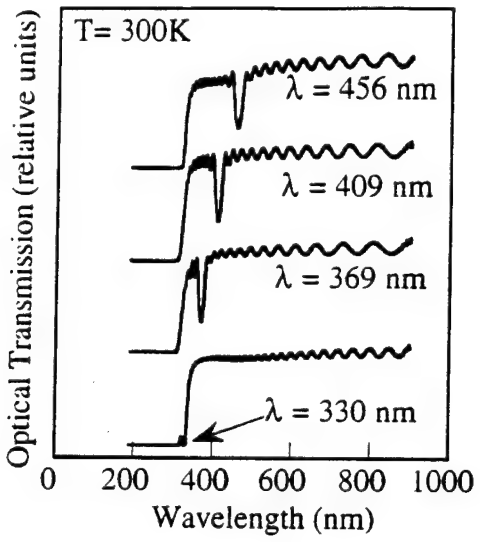

Figure 6. Room temperature optical transmission of selected Bragg reflectors using $\{Al_{0.5}Ga_{0.5}N / Al_{0.2}Ga_{0.8}N\}$ multilayers

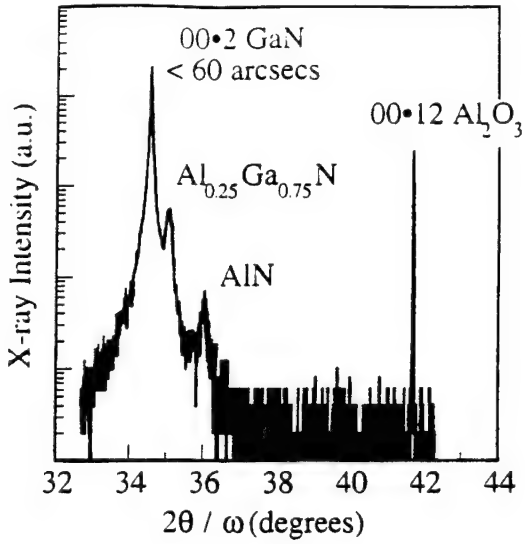

Figure 7. X-ray diffraction spectrum of a $Al_{0.25}Ga_{0.75}N$:Si / GaN structure exhibiting 2 DEG.

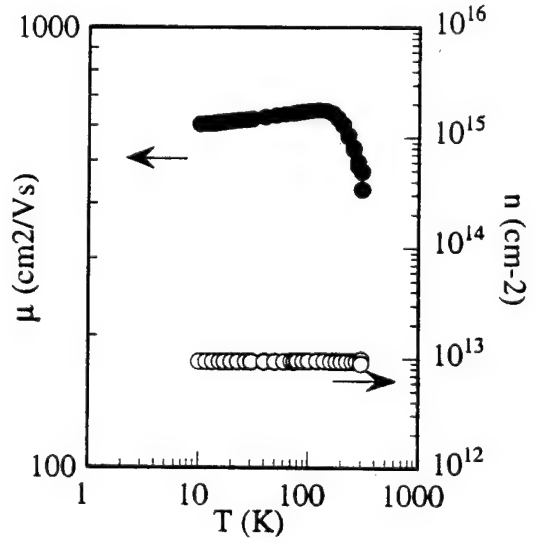

Figure 8. Temperature dependent Hall data for a $Al_{0.25}Ga_{0.75}N$:Si / GaN structure exhibiting 2DEG.

III.7. Two Dimensional Electron Gas in $Al_xGa_{1-x}N$-GaN Heterostructures

In order to determine and improve the quality of our heterostructure interfaces, we attempted to achieve two dimensional electron gas in $Al_xGa_{1-x}N$:Si / GaN structures on basal plane sapphire substrates. More precisely, a 0.7 μm thick insulating GaN was first grown on the AlN buffer layer. Then a ~30 Å thick undoped $Al_{0.25}Ga_{0.75}N$ was grown, followed by a ~570Å thick Si-doped $Al_{0.25}Ga_{0.75}N$ electron emitter layer. These thicknesses and the ternary composition were arbitrarily chosen. A typical X-ray diffraction spectrum of this structure is shown in Figure 7. The electrical properties, as determined by Hall measurements as a function of temperature, are shown in Figure 8. The sheet carrier density was constant near 10^{13} cm^{-3}, while the mobility increased up to 600 cm^2/Vs when the temperature was reduced. This behavior of the sheet carrier density and mobility clearly demonstrate the presence of a two dimensional electron gas in this structure.

A more recent sample exhibited mobilities of ~1000 cm^2/Vs and 2000 cm^2/Vs at 300K and 77K respectively, but the temperature dependent electrical measurements were not measured. These mobilities are still lower than those reported recently [11], but the results presented here were obtained on unoptimized structures. More optimization is needed to further enhance the carrier mobility.

III.8. $Al_xGa_{1-x}N$ / GaN Superlattices

To further characterize our $Al_xGa_{1-x}N$ / GaN structures, we grew a few superlattices and structurally characterized them with X-ray diffraction and transmission electron microscopy. The X-ray diffraction spectrum of a superlattice consisting of 13 period {500Å $Al_{0.2}Ga_{0.8}N$ / 50Å GaN} structure grown on a sapphire substrate exhibited two main peaks corresponding to the bulk GaN layer and the $Al_{0.2}Ga_{0.8}N$ layers, as shown in Figure 9. The widths of these peaks were about 100 arcsecs. Satellite peaks can be clearly observed up to the tenth peak, confirming the excellent quality of the films and interfaces. A further confirmation can be achieved using TEM analysis, which has already been discussed in Section II.

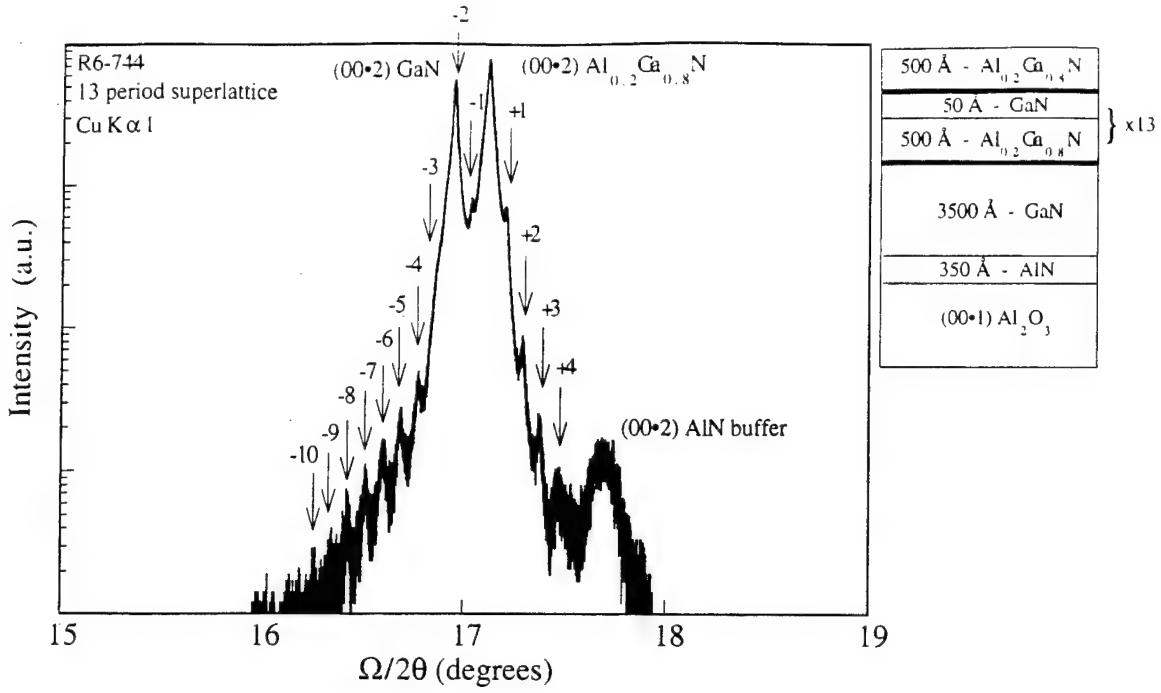

Figure 9. "Open detector mode" X-ray diffraction spectrum of a 13 period {500Å $Al_{0.2}Ga_{0.8}N$ / 50Å GaN} superlattice grown on a sapphire substrate.

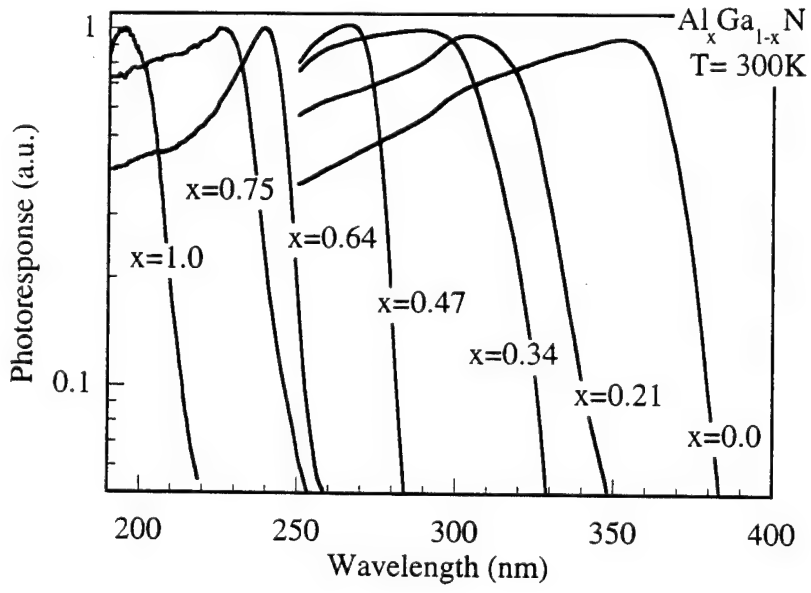

Figure 10. Room temperature normalized photoresponse of $Al_xGa_{1-x}N$ photodetectors.

III.9. $Al_xGa_{1-x}N$ Ultraviolet Photoconductors

Our success in achieving high quality $Al_xGa_{1-x}N$ alloys allowed us to realize ultraviolet photodetectors with various cut-off wavelengths. The photoconductors were fabricated using the $Al_xGa_{1-x}N$ epilayers (0.5 to 1.5 μm) deposited as described previously. Metal contacts were deposited onto the film to realize low resistance ohmic contacts. The spectral responsivity of these devices was measured using a Xe arc lamp, focused into a monochromator after an optical chopper. The detector was placed at the exit of the monochromator and a standard synchronous detection scheme was used. The spectral power of the Xe lamp was calibrated using a Si ultraviolet photodetector.

Figure 10 shows the normalized photoresponse of these detectors. The cut-off wavelengths can be clearly tailored from 365 nm to 200 nm with the alloy composition. To the best of our knowledge, this is the only report of photodetectors with cut-off wavelengths as low as 200 nm, using III-Nitride materials.

III.10. Conclusions

In conclusion, we have reported the MOCVD growth, n-type and p-type doping and characterization of $Al_xGa_{1-x}N$ alloys on sapphire substrates. We have presented the fabrication of $Al_xGa_{1-x}N$ based Bragg reflectors with controlled peak reflectivity wavelength and the demonstration of two dimensional electron gas in III-Nitrides. $Al_xGa_{1-x}N$ / GaN heterostructures and superlattices exhibited sharp interfaces and clear satellite peaks in the X-ray diffraction spectrum. Finally, we have demonstrated $Al_xGa_{1-x}N$ based UV photodetectors with tailored cut-off wavelengths from 365 to 200 nm.

III.11. References

[1]. A. Saxler, P. Kung, C.J. Sun, E. Bigan, and M. Razeghi, Appl. Phys. Lett. **64**, 339 (1994).

[2]. P. Kung, A. Saxler, X. Zhang, D. Walker, T.C. Wang, I. Ferguson, and M. Razeghi, Appl. Phys. Lett. **66**, 2958 (1995).

[3]. X. Zhang, P. Kung, D. Walker, A. Saxler, and M. Razeghi in Gallium Nitride and Related Materials, edited by F.A. Ponce, R.D. Dupuis, S. Nakamura, and J.A. Edmond (Mater. Res. Soc. Proc. **395**, Pittsburgh, PA, 1996) pp. 625-629.

[4]. X. Zhang, D. Walker, A. Saxler, P. Kung, J. Xu, and M. Razeghi, Electron. Lett. **32**, 1622 (1996).

[5]. X. Zhang, P. Kung, D. Walker, J. Piotrowski, A. Rogalski, A. Saxler, and M. Razeghi, Appl. Phys. Lett. **67**, 2028 (1995).

[6]. P. Kung, X. Zhang, D. Walker, A. Saxler, J. Piotrowski, A. Rogalski, and M. Razeghi, Appl. Phys. Lett. **67**, 3792 (1995).

[7]. K. Hiramatsu, T. Detchprohm, and I. Akasaki, Jpn. J. Appl. Phys. **32**, 1528 (1993).

[8]. T.J. Kistenmacher, D.K. Wickenden, M.E. Hawley, and R.P. Leavitt, Appl. Phys. Lett. **67**, 3771 (1995).

[9]. H. Murakami, T. Asahi, H. Amano, K. Hiramatsu, N. Sawaki, and I. Akasaki, J. Cryst. Growth **115**, 648 (1991).

[10]. S. Yoshida, S. Mizawa, and S. Gonda, J. Appl. Phys. **53**, 6844 (1982).

[11]. M.A. Khan, Q. Chen, C.J. sun, M. Shur, and B. Gelmont, Appl. Phys. Lett. **67**, 1429 (1995).

[12]. M. Razeghi, presented at the International Symposium on Nitrides, St. Malo, France, 1996 (unpublished).

IV. CHARACTERIZATION OF ULTRAVIOLET PHOTODETECTORS

IV.1. Introduction

GaN, AlN and their alloys $Al_xGa_{1-x}N$ are promising materials for developing ultraviolet (UV)-visible optoelectronic devices because of their direct bandgaps and relatively high mobilities. In addition, the ternary materials are desirable for developing high performance optoelectronic devices utilizing heterostructures. By changing the Al-composition, x, from 0 to 1, the energy gap of this ternary material can be tuned from 3.4 eV to 6.2 eV, which spans the wavelengths from 365 nm to 200 nm. In particular, it includes the strategic window (230 nm to 280 nm) of ozone layer absorption. The intrinsic solar blindness of these detectors leads to applications in the aerospace, automotive and petroleum industries. We have previously reported the fabrication of $Al_xGa_{1-x}N$ UV photoconductors with cut-off wavelengths down to 260 nm [1]. Here, we report the noise and carrier lifetime measurements of $Al_xGa_{1-x}N$ ($0 \leq x \leq 1$) photodetectors with an extended range of cut-off wavelengths from 365 nm to 200 nm.

IV.2. $Al_xGa_{1-x}N$ Material

$Al_xGa_{1-x}N$ epitaxial layers have been grown on basal plane sapphire by metalorganic chemical vapor deposition (MOCVD). A thin AlN layer was deposited at high temperatures prior to the growth of $Al_XGa_{1-X}N$ layers, which were undoped. The thicknesses of the $Al_xGa_{1-x}N$ epitaxial layers were about 1 mm. Trimethylgallium (TMGa), triethylgallium (TEGa), trimethylaluminum (TMAl), and ammonia were used as source materials for the Ga, Al, and N elements, respectively. The alloy composition was adjusted by varying the flow ratios of TMGa, TEGa and TMAl. Detailed growth conditions have been reported in a previously [2]. All of the samples were transparent, smooth, and free of cracks. The samples were all semi-insulating. Figure 1 shows the optical transmission of the $Al_xGa_{1-x}N$ ($0 \leq x \leq 1$) layers, which were measured with a Varian Cary-13E dual-beam UV spectrometer at room temperature. The transmission ranges from 200 nm to 365 nm with sharp cut-off edges. The Fabry-Perot interference fringes displayed in the optical transmission curves confirms the presence of a smooth and uniform surface morphology.

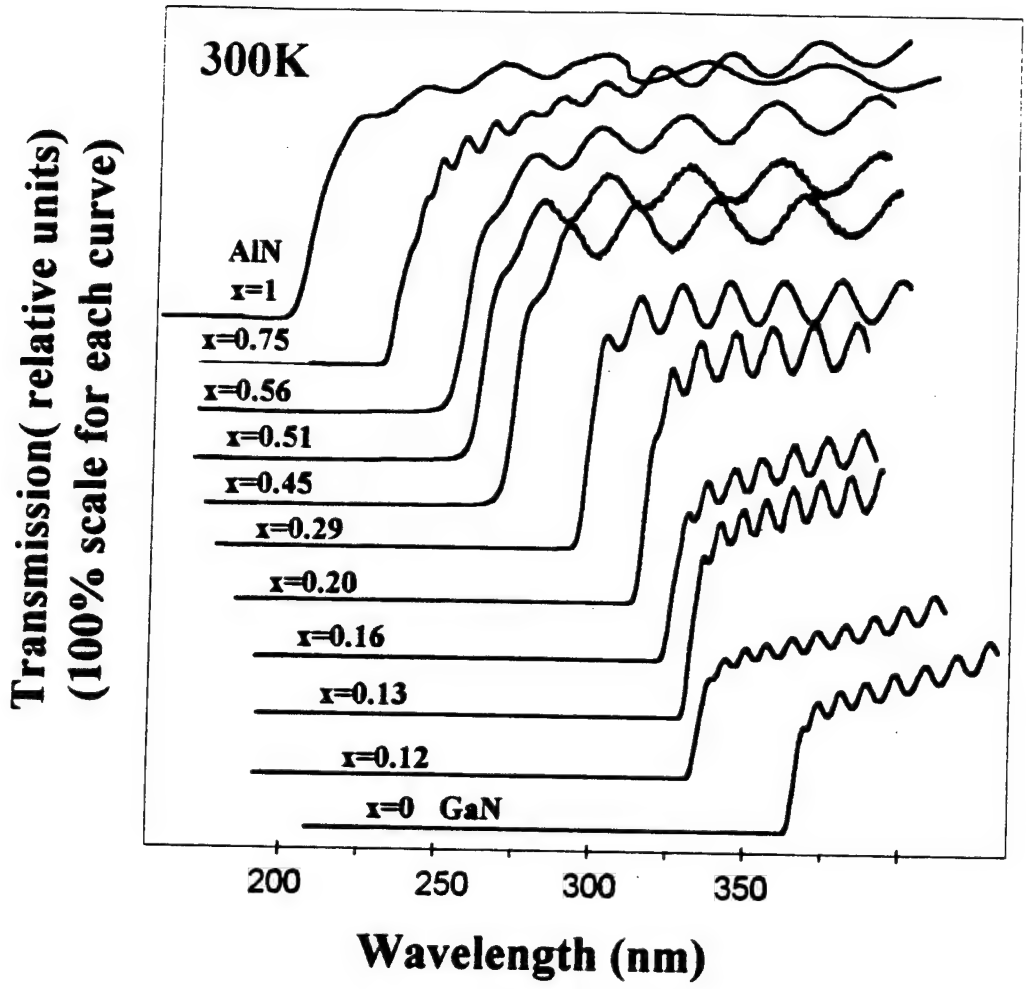

Figure. 1. The optical transmission of $Al_xGa_{1-x}N$ ($0 \leq x \leq 1$) layers grown by MOCVD.

IV.3. Detectors

The photoconductive detectors were fabricated using two indium stripe contacts with a separation of 1 mm and a length of 4 mm. The contacts were blocked from illumination so that the influence of any possible photoelectric effect would be minimized. The light source was an OSRAM 75W Xenon lamp with a normal quartz glass window that allows emission down to ~170 nm. In order to determine the spectral response of the photoconductors, the Xe lamp light was chopped at 14 Hz and focused into a monochromator. The photoconductors were placed at the exit slit of the monochromator. The rest of the biasing circuit was contained in an electrically isolated box to eliminate any electromagnetic interference. A synchronous detection scheme was used to measure the detector signal. This monochromator has a focal length of 27.5 cm and is equipped with a holographic grating with blaze wavelength at 250 nm, thus ensuring good efficiency to very short wavelengths. The photoconductor was in series with a load resistor, R_L. Because of the large resistance of the photoconductors, they were operated in the constant-voltage mode. A Si UV photodetector was used to calibrate the power of the Xenon lamp. The noise measurements were taken with a SR760 FFT Spectrum Analyzer (Stanford Research Systems) at room temperature. The setup and conditions for these measurements were kept identical to those which the system was under during the measurements of the response with the exception of the placement of the sample. During the noise measurements, the sample was kept in the box with the rest of the biasing circuit so that it would be shielded from any light.

IV.4. Results

The responsivity linearly increases with bias voltage. It eventually saturates at high voltages due to the sweep out effect [3]. The noise is found to decrease with increasing frequency, while leveling off around 30 kHz and remaining flat at high frequencies . For low Al-composition $Al_xGa_{1-x}N$ photodetectors, the high-frequency noise is limited by Johnson noise. The noise of the AlN photodetectors is higher than their Johnson noise.

Based on the responsivity and noise measurements, the detectivities were calculated using the following equation:

$$D^* = \frac{R_p}{i_n / \sqrt{\Delta f}} \sqrt{A} \qquad (1)$$

where R_v is the responsivity, $i_n/\sqrt{\Delta f}$ is the power spectral density of the noise signal, and A is the area of the detector. Figure 2 shows the detectivity of $Al_xGa_{1-x}N$ ($0 \le x \le 1$) UV photodetectors at a modulating frequency of 14 Hz. The peak detectivities are in the range of 3.81×10^7 - 5.5×10^8 cm·Hz$^{1/2}$/W, as displayed in Table I with the corresponding Al content and cutoff wavelength. Below the bandgap wavelength, the detectivity linearly increases with increasing wavelength, whereas near the bandgap, it exhibits a sharply decreasing responsivity. This indicates that the detector has high quantum efficiency up to the cut-off wavelength.

In an attempt to correlate the detectivity with the carrier lifetime we studied the kinetics of photoconductivity, as done in our previous work, by measuring the frequency-dependent photoresponse [4]. The responsivities for all $Al_xGa_{1-x}N$ photodetectors decrease dramatically with increasing frequency at low frequencies and reach a constant at high frequencies. Figure 3 shows a typical frequency-dependent photoresponse of an $Al_xGa_{1-x}N$ photodetector. Taking the chopper modulation into consideration, which can be approximated as a square modulation, the frequency-dependent response can be described by the following equation:

$$R_v(f) = \left(\frac{q\lambda\eta}{hc}\right) R_L \left(\frac{\mu_e \tau_{eff} V_b}{\ell^2}\right) \tanh\left(\frac{1}{4\tau_{eff} f}\right) \qquad (2)$$

where η is the quantum efficiency, μ_e is the electron mobility, λ is the wavelength of the incident light, ℓ is the electrode spacing, V_b is the DC bias voltage across the photoconductor, f is the modulation frequency and τ_{eff} is the effective majority carrier lifetime. The latter, obtained from the frequency-dependent photoresponse, is between 6 ms and 35 ms, as shown in the following Table. It increases with increasing Al-composition in $Al_xGa_{1-x}N$ materials. This may be attributed to the influence of deep-level traps in higher Al-composition samples. One mechanism that has been proposed to occur in high Al-content ternary materials involves the appearance of a trapping layer as the Al concentration is increased [5].

Detector active layer $Al_xGa_{1-x}N$	λ cutoff (nm)	D^*_{peak} (cmHz$^{1/2}$/W)	τ_{eff} (ms)
x = 0	365	5.54×10^8	6
x = 0.75	230	3.33×10^8	25
x = 1	200	3.81×10^7	35

Table I. The detectivity and majority carrier lifetime of $Al_xGa_{1-x}N$ ($0 \le x \le 1$) photodetectors.

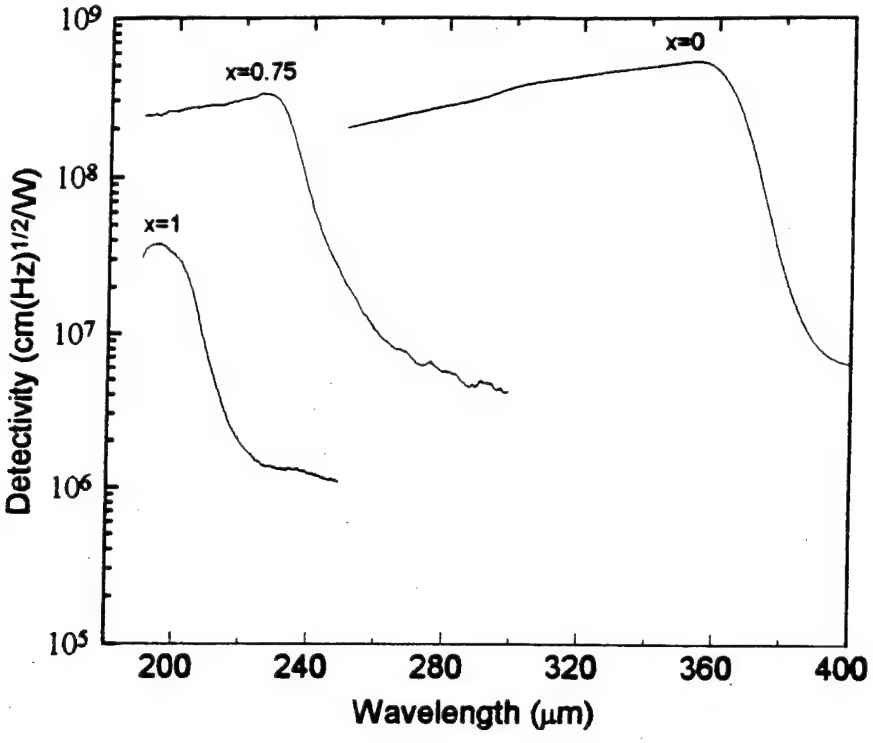

Figure 2. The detectivity of $Al_xGa_{1-x}N$ ($0 \leq x \leq 1$) photodetectors at a modulating frequency of 14 Hz.

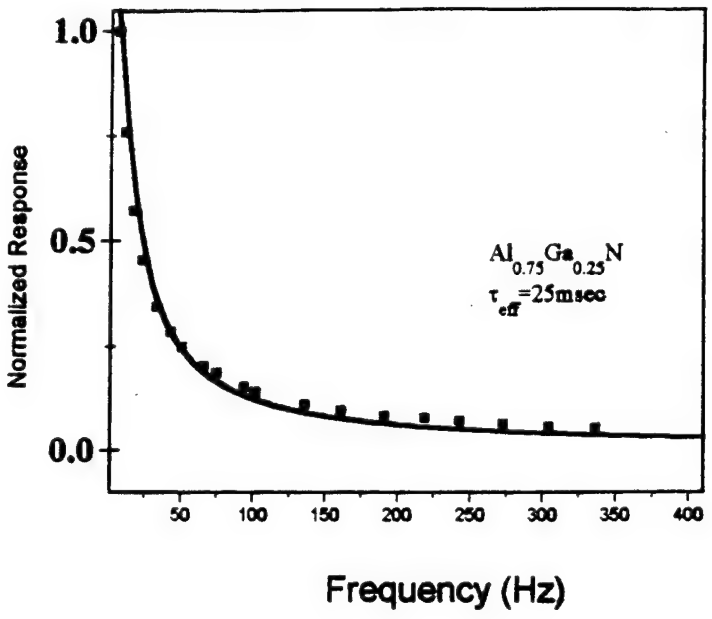

Figure 3. Frequency-dependent response of $Al_{0.75}Ga_{0.25}N$ photodetector.

IV.5. Conclusions

In conclusion, we have successfully demonstrated the feasibility of $Al_xGa_{1-x}N$ photoconductors with cut-off wavelengths from 365 nm to 200 nm. The maximum detectivity at 14 Hz is 5.5×10^8 cm·Hz$^{1/2}$/W. The carrier lifetime derived from frequency-dependent responsivity measurements is in the range from 6 to 36 ms. These high sensitivity photodetectors along with their wide range of cut-off wavelengths from 365 nm to 200 nm provide an advancement to the prospective future of UV optoelectronics.

The next step will be to improve the performance of these detectors by optimizing their geometry through extensive use of the etching system to be installed in January 1997. Moreover, further improvement in the optical and electrical properties of the $Al_xGa_{1-x}N$ material used will also be sought.

IV.6. References

[1] D. Walker, X. Zhang, P. Kung, A. Saxler, S. Javadpour, J. Xu, and M. Razeghi, Appl. Phys. Lett. **68**, 2100(1996)

[2] X. Zhang, P. Kung, A. Saxler, D. Walker, T. C. Wang and M. Razeghi, Appl. Phys. Lett. **67**, 1745 (1995).

[3] M. Razeghi, A. Rogalski, Infrared Photon Detectors J. Appl. Phys. **79**, 7433 (1996).

[4] P. Kung, X. Zhang, D. Walker, A. Saxler, J. Piotrowski, A. Rogalski, and M. Razeghi, Appl. Phys. Lett. **67**, 3792 (1995).

[5] D. W. Jenkins, J. Appl. Phys. **72**, 4130 (1992).

V. NOVEL SUBSTRATES:
MOCVD GROWTH OF GaN THIN FILMS ON β-$LiGaO_2$ substrates

V.1. Introduction

GaN and its alloys are ideal semiconductor materials for photonic devices operating in the visible-near UV spectral region. In a series of papers, we have already reported the metalorganic chemical vapor deposition (MOCVD) and characterization of high quality AlN, GaN and $Al_xGa_{1-x}N$ thin films on sapphire (α-Al_2O_3) substrates [1-5], as well as demonstrated GaN-based photovoltaic and photoconductive detectors on sapphire substrates.[6-8]

These results have been obtained in spite of the large lattice mismatch between GaN and Al_2O_3 (~16%). The on-going effort to improve the GaN film properties has driven the research community to look for an alternative and better substrate material than sapphire. Although synthesized as early as in 1965, it is only recently that the beta phase of lithium gallate (β-$LiGaO_2$ or LGO) has received attention because it is a promising new substrate material which is quasi-lattice matched to GaN. Here, we discuss the advantages of LGO over Al_2O_3 and we describe the MOCVD growth and characterization of single crystal GaN thin films on LGO substrates.

V.2. Crystal structures and physical properties of LGO

A comparison of the physical properties of GaN, Al_2O_3 and LGO is given in Table I below. The structure of LGO is similar to the wurtzite structure. However, because Li and Ga atoms have different sizes, β-$LiGaO_2$ is not a wurtzite crystal but is orthorhombic.[9] The (001) face contains either oxygen anions or group-III cations. The atomic arrangement in this (001) face is hexagonal-like, which promotes the epitaxial growth of the (00•1) of GaN in order to match the hexagonal symmetry in these two planes. One would thus expect the following epitaxial relationship: (00•1) GaN / (001) LGO. The distance between nearest cations in LGO is in the range of 3.133-3.189 Å, while the distance between nearest anions is in the range of 3.021-3.251 Å.[10] The lattice mismatch between (00•1) GaN on (001) LGO is then 1-2 %, which is the lowest value among all available substrate materials.

	wurtzite GaN	α-Al_2O_3	β-$LiGaO_2$ [9,10]
Crystal symmetry	hexagonal	trigonal	orthorhombic
Space group	$P6_3mc$ (No. 186)	R-$3c$ (No. 167)	$Pna2_1$ (No. 33)
Lattice constants (Å)	a = 3.189	a = 4.758	a = 5.402
	c = 5.185	c = 12.991	b = 6.372
			c = 5.007
Melting point (°C)	sublimes	2030	1600
Substrate orientation used for epitaxy		(00•1)	(001)
Lattice mismatch	0 %	16.1 %	1-2 %

Table I. Comparison of the physical properties of GaN, α-Al_2O_3 and β-$LiGaO_2$.

In our previous work [11], we discussed the formation of edge-type dislocations at the substrate-film interface to accommodate any lattice mismatch. Applying this to the case of LGO, we can easily show that the density of such dislocations would be more than 2 orders of magnitude smaller at the (00•1) GaN / (00•1) LGO interface than at the (00•1) GaN / (00•1) Al_2O_3 interface. Consequently, LGO appears to be a very promising substrate material for the growth of GaN epilayers because they would have much fewer defects and improved properties than the films grown on Al_2O_3.

However, to date, the potential of LGO as an alternative substrate to sapphire for the growth of GaN thin films has not yet been proven. It has been suggested that using LGO is more challenging than Al_2O_3 because of its low melting point and its high sensitivity to hydrogen and water.[12] Little is known about the LGO substrate physical properties, its cleaning procedures and its stability during epitaxial growth. The only approach in order to address these issues is then to conduct the epitaxial growth and characterization of GaN thin films on LGO, which is the object of this study reported here.

V.3. Experimental

The LGO substrates in this study were used as received from the manufacturer.[13] The GaN epilayers were grown in a low pressure MOCVD reactor as described earlier.[3] In this study, the growth temperature was varied from 600 to 1000 °C. Purified nitrogen was used as the

carrier gas. The NH_3 flow rate was 200 sccm. The Ga molar flow rate was kept at ~40 μmol/min. yielding a growth rate of ~ 0.7 μm/hr as determined by cross-section scanning electron microscopy (SEM). The films were grown directly on (001) LGO without any buffer layer. They were characterized by SEM, X-ray diffraction, Hall measurement, photoluminescence and optical absorption.

V.4. Characterization results

Figure 1 shows SEM micrographs of the surface morphologies of LGO substrates prior to growth as well as the GaN overlayers grown between 600 to 900 °C. At 600 °C, the film surface morphology was very rough, demonstrating that the growth at this temperature was not oriented. At 700 °C, the growth became quasi two-dimensional and the films were much smoother. For T_g = 800 and 900 °C, the films were smooth, with some grooves and holes due to the incomplete coalescence of GaN during the layer-by-layer growth. This shows that the surface diffusion of adatoms during growth was high enough at 700 °C in order to achieve two dimensional growth. The films grown at 1000 °C started peeling off as soon as they were in contact with the water vapor in ambient atmosphere. This suggests that the LGO substrates were damaged during the high temperature growth and became reactive with water, which reduced the adherence of the GaN epilayers. A growth temperature of 1000 °C is thus too high when using LGO substrates. These samples could not be further characterized.

Basal plane sapphire substrates have also been used along with LGO for each of the growths. The substrate preparation procedure has been reported earlier.[3] For all of the growth conditions employed, the single-step GaN grown on Al_2O_3 was discontinuous, forming islands and columnar structures similar to those reported by Hiramatsu *et al* [14] Figure 1(f) is a typical SEM micrograph of a GaN grown on (00•1) Al_2O_3 which demonstrates that the single-step growth of GaN on (00•1) Al_2O_3 is always three dimensional in the conditions employed.

X-ray diffraction measurements were conducted for the GaN films grown on (001) LGO and showed the epilayers crystallized in the wurtzite phase. The epitaxial relationship predicted by the crystallographic model was also confirmed: (00•1) GaN / (001) LGO. Figure 2 shows the X-ray rocking curve of the GaN films (00•2 reflections) as a function of T_g. The films grown at 600 °C were polycrystalline. Above 700 °C, the films were single crystalline with rocking curve linewidths from 1000, 700 and 300 arcsecs as shown in Figure 3(a). The low linewidth of 300 arcsecs is similar to what has commonly obtained for GaN on sapphire until recently.[15]

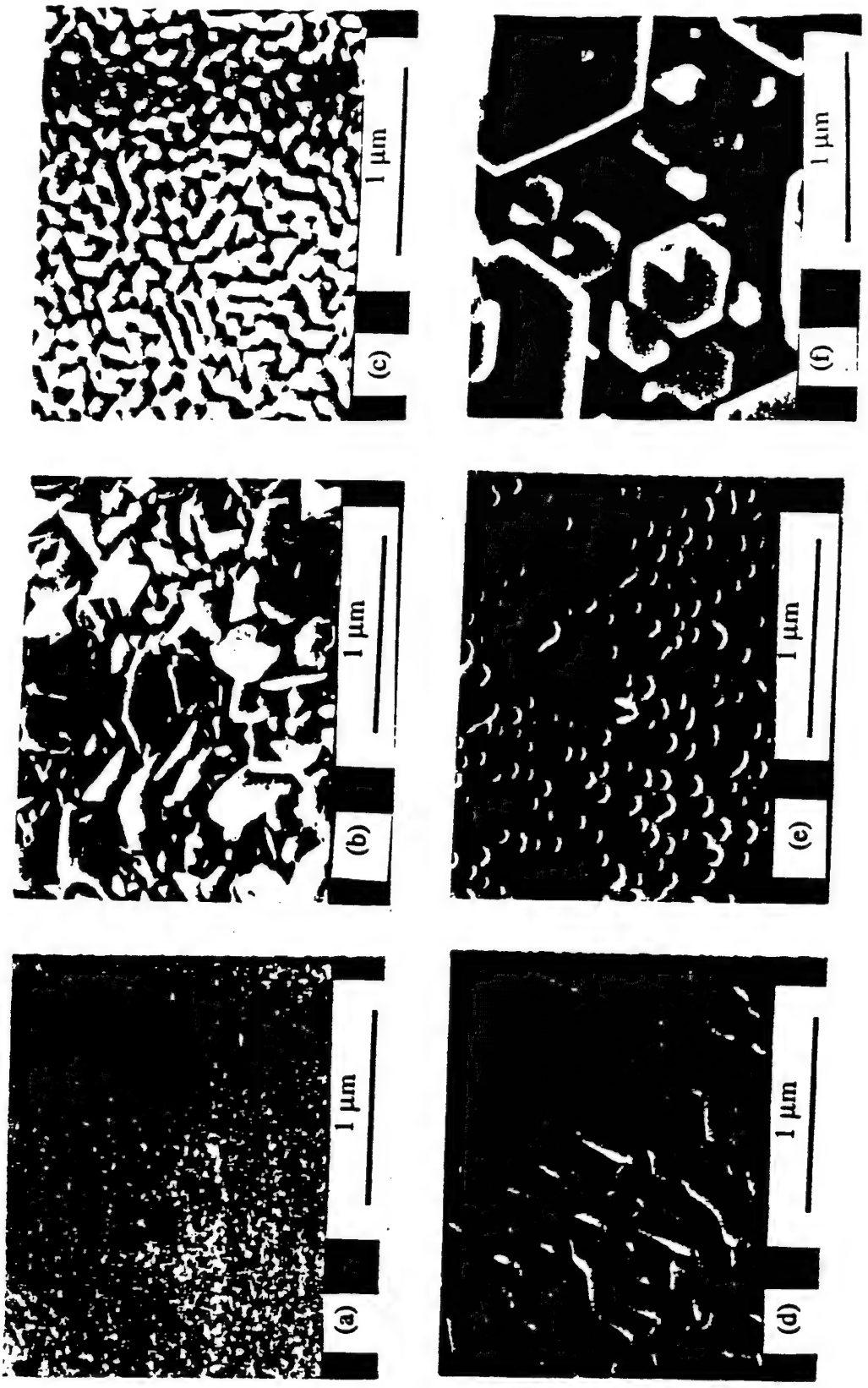

Figure 1. SEM micrographs of (a) (001) β-$LiGaO_2$ prior to deposition, of GaN grown on (001) β-$LiGaO_2$ at (b) 600 °C, (c) 700 °C, (d) 800 °C and (e) 900 °C, of GaN grown on (00•1) Al_2O_3 at 900 °C.

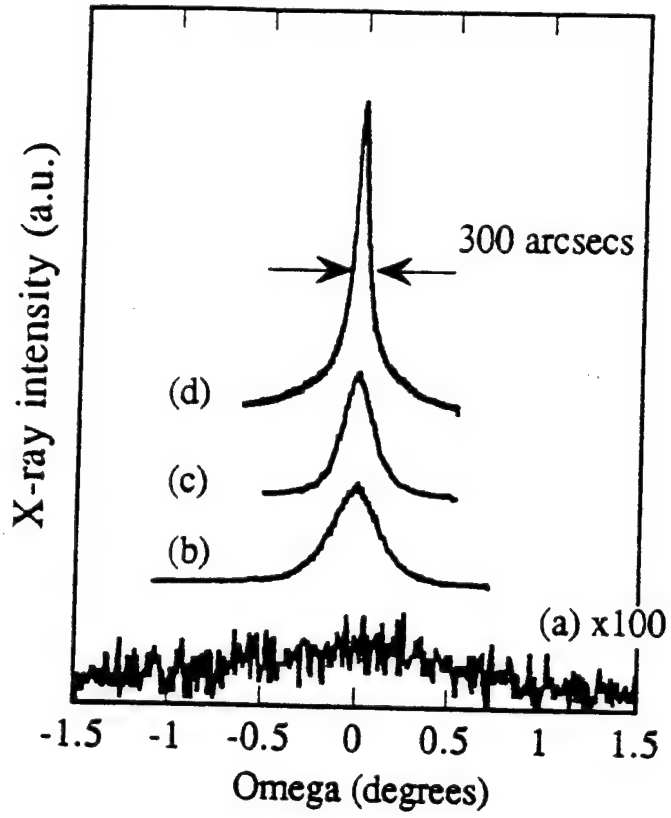

Figure 2. X-ray rocking curve of GaN grown on β-$LiGaO_2$ at (a) 600 °C, (b) 700 °C, (c) 800 °C and (d) 900 °C.

These results show that high quality monocrystalline GaN films can be grown on LGO substrates at temperatures as low as 700 °C, which are ~ 300 °C lower than those commonly used on sapphire substrates.[3]

All the GaN layers grown on LGO were n-type ($n \sim 1 \times 10^{20}$ cm^{-3}) as determined by room temperature Hall measurements. The electron mobility was ~10 cm^2/Vs. The high electron concentrations may be due to the incorporation of oxygen, resulting from the decomposition of LGO at elevated temperatures.

Figure 4(a) shows a typical room temperature optical transmission of GaN films grown on LGO at $T_g \geq 700$ °C. The spectrum was measured by a visible-UV spectrometer using a two-beam technique. Fabry-Perot type oscillations in the transmission spectrum confirm the smoothness of the film surface morphology. The short-period oscillations in the spectrum are due to the thickness difference between the LGO substrate used as the reference and the one on which the measurement sample was grown. A sharp absorption edge can be determined at ~3.60 eV. Figure 4(b) shows a typical room temperature photoluminescence spectrum of GaN films grown on LGO at $T_g = 700$ °C. Intense luminescence emission was detected near the bandedge of GaN at 3.44 eV with a linewidth of ~180 meV. A broad and less intense yellow emission band could also be detected at ~2.3 eV, due to the presence of deep-levels in the bandgap.

The near-bandedge luminescence peak was detected at an energy ~40 meV higher than the bandgap energy (3.4 eV). Generally, in highly doped semiconductors, there is a blue shift of the photoluminescence peak because the Fermi level lies inside a band.[16] With a carrier concentration on the order of 10^{20} cm^{-3}, which is nearly 40 times higher than $N_c \approx 2.59 \times 10^{18}$ cm^{-3}, the Fermi level is expected to be more than 250 meV above the bottom of the conduction band.[17] Such a high value cannot account for the 40 meV blue shifted luminescence peak. The interpretation of this blue shift is still under investigation.

In Figure 3(b) and 3(c), we compared the bandedge and the yellow emission intensities as a function of the growth temperature. The measurements were carried out in the same conditions. A maximum of the near bandedge emission was obtained for $T_g = 700$ °C. For T_g below 700 °C, both the near bandedge and the yellow luminescence emissions were weak because of the poor crystalline quality of the films. For T_g above 700 °C, the bandedge luminescence also decreased, but the intensity of the yellow luminescence significantly increased with higher growth temperatures. This shows that the electron-hole recombination mechanisms occurred predominantly through deep-levels rather than between near bandedge states. We have not

observed such behavior for GaN films grown on sapphire, which suggests that the origin of these deep-levels is related to the use of LGO substrates. Deep-levels may arise from the combination of impurity-related and structural defects. Pankove *et al.* have observed a strong photoluminescence peak at ~2.23 eV at room temperature from Li-doped GaN on sapphire.[18] In our case, the incorporation of Li into GaN was most likely as a result of the decomposition of the β-$LiGaO_2$ substrates at elevated temperatures. However, we cannot rule out the contribution due to structural defects.

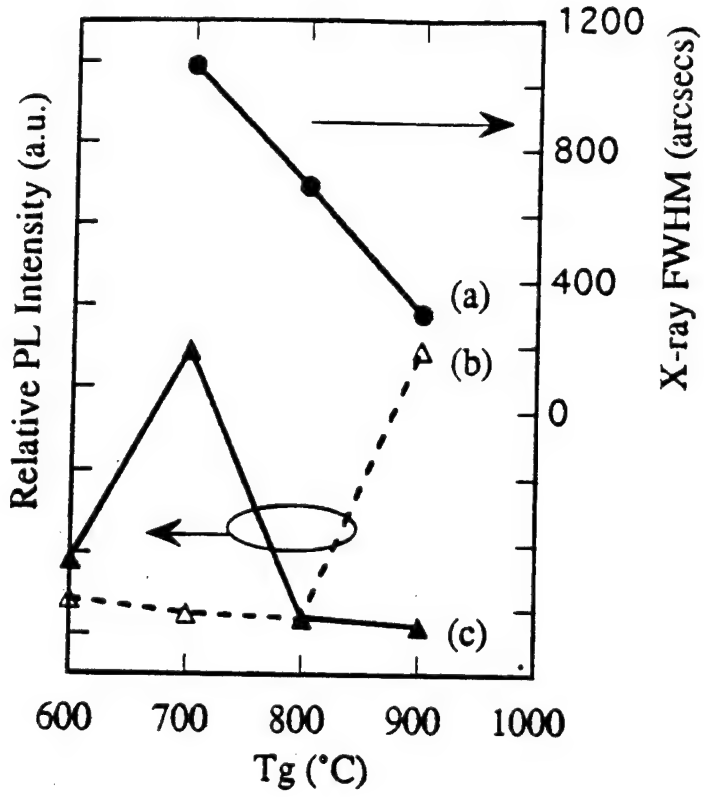

Figure 3. (a) X-ray rocking curve FWHM, (b) yellow photoluminescence and (c) near bandedge photoluminescence intensity of GaN grown on β-$LiGaO_2$ as a function of growth temperature.

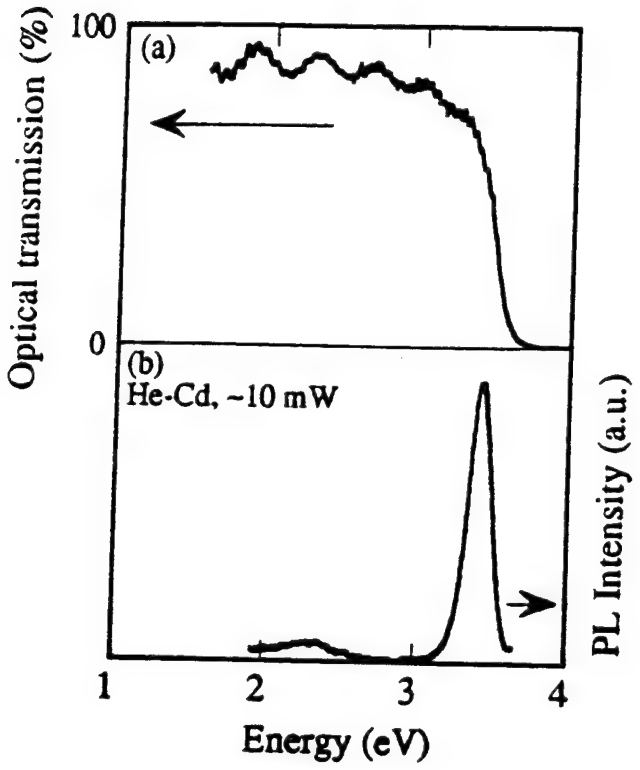

Figure 4. Typical room temperature (a) optical transmission and (b) photoluminescence of GaN films grown on β-$LiGaO_2$ at T_g = 700 °C.

V.5. Conclusion

We have shown that β-$LiGaO_2$ is a promising substrate material for the growth of GaN thin films. Single crystal GaN was grown on LGO substrates by MOCVD, with smooth surface morphologies and X-ray rocking curve as narrow as 300 arcsecs for T_g = 900 °C. Near bandedge photoluminescence was the most intense for samples grown at 700 °C. The peak was detected at 3.44 eV, which is at a higher energy than the expected bandgap energy.

However, more work is needed in order to achieve GaN films on LGO with the same quality as the best ones grown on Al_2O_3. One important area of future investigation will be the use of a GaN buffer layer prior to the growth of single crystal GaN on LGO.

V.6. References

[1] C.J. Sun and M. Razeghi, Appl. Phys. Lett. **63**, 973 (1993).

[2] A. Saxler, P. Kung, C.J. Sun, E. Bigan, and M. Razeghi, Appl. Phys. Lett. **64**, 339 (1994).

[3] P. Kung, A. Saxler, X. Zhang, D. Walker, T.C .Wang, I. Ferguson, and M. Razeghi, Appl. Phys. Lett. **66**, 2958 (1995).

[4] X. Zhang, P. Kung, A. Saxler, D. Walker, T. Wang, and M. Razeghi, Acta Phys. Pol. **88**, 601 (1995).

[5] X. Zhang, P. Kung, A. Saxler, D. Walker, T.C. Wang, and M. Razeghi, Appl. Phys. Lett. **67**, 1745 (1995).

[6] X. Zhang, P. Kung, D. Walker, J. Piotrowski, A. Rogalski, A. Saxler, and M. Razeghi, Appl. Phys. Lett. **67**, 2028 (1995).

[7] P. Kung, X. Zhang, D. Walker, A. Saxler, J. Piotrowski, A. Rogalski, and M. Razeghi, Appl. Phys. Lett. **67**, 3792 (1995).

[8] D. Walker, X. Zhang, P. Kung, A. Saxler, S. Javadpour, J. Xu, and M. Razeghi, Appl. Phys. Lett. **68**, 2100 (1996).

[9] M. Marezio, Acta Cryst. **18**, 481 (1965).

[10] P. Kung, A. Saxler, X. Zhang, D. Walker, and M. Razeghi (unpublished).

[11] C.J. Sun, P. Kung, A. Saxler, H. Ohsato, K. Haritos, and M. Razeghi, J. Appl. Phys. **75**, 3964 (1994).

[12] B. Chai, private communication.

[13] Supplied by Crystal Photonics Inc., Oviedo, FL.

[14] K. Hiramatsu, S. Itoh, H. Amano, I. Akasaki, N. Kuwano, T. Shiraishi, and K. Oki, J. Cryst. Growth **115**, 68 (1991).

[15] J.N. Kuznia, M.A. Khan, D.T. Olson, R. Kaplan, and J. Freitas, J. Appl. Phys. **73**, 4700 (1993).

[16] J.I. Pankove, in *Optical Process in Semiconductors* (Dovers Publications, NY, 1971).

[17] H. Nakayama, P. Hacke, M.R.H. Khan, T. Detchprohm, K. Hiramatsu, and N. Sawaki, Jpn. J. Appl. Phys. **35**, L282 (1996).

[18] J.I. Pankove, M.T. Duffy, E.A. Miller, and J. Bei-rkeyheiser, J. Lumin. **8**, 89 (1973).

VI. DRY ETCHING: A REVIEW

VI.1. Introduction

In this section, we present a survey of the state-of-the-art of dry etching of III-V nitrides reported in the literature. The purpose of this survey was to help us ramp-up our dry etching capabilities at the Center for Quantum Devices once the etching system was installed in January 1997. In the next section (VII), we will present our preliminary results on the dry etching of GaN based materials using a PlasmaTherm 770 Dry Etching System, as well as the photovoltaic and electroluminescence characterization of a simple GaN p-i-n junction mesa structure.

In this survey, the dependence of the etch rates on rf power, process pressure, microwave power, material quality, electrode temperature, etchant concentration and plasma chemistry are discussed. The structural and electrical damages on the samples resulting from dry etching are also discussed.

There has been much experimentation with different plasma chemistries for dry etching the III-V nitrides. This is necessary because of the resilience that these materials have shown during wet chemical etching. It has been conclusively shown that etch rates under high ion density conditions, such as in electron cyclotron resonance (ECR) and magnetron-enhanced reactive ion etching (MIE), are much higher than for conventional reactive ion etching (RIE). But furthermore, the highest etch rates (~4000Å/min) for III-nitrides with these improved conditions are still slower by a factor of 3-5 than conventional III-V's like GaAs under the same conditions [1]. For some chemistries this effect is even more pronounced. For instance, GaN etches ~50 times slower than GaAs for the same plasma conditions using $SiCl_2$/Ar, because highly energetic ions are needed to break the strong chemical bond of GaN [2]. The benefit of using ECR is that by superimposing a rf bias on the sample, the ion density can be controlled independent of the ion energy. All of the work mentioned in this report are from groups who utilized a standard ECR system for dry etching.

One thing that we will have to take into consideration while contemplating the previous results achieved in this field is the crystal quality of the samples that were tested. Many of the results come from the same research group and who seem to be consistently using material which is "single crystal with a high density of stacking faults and microtwins" [3]. Logic and previous tests agree that the material quality significantly affects the etch rate.

VI.2. Etch rates

There are many things which affect the etch rate, including the most obvious, the chemistry of the plasma; among these rest are: rf power (which affects the dc bias), process pressure and microwave power (both of which affect the ion current density), electrode temperature, material quality, and percent of active chemical species in the discharge. To clarify the findings, the results will be listed under the specific etch rate influence.

VI.2.1. RF power (dc bias)

The rf power etch rate dependence was investigated by Zhang *et. al.* during a study of the effects of etching GaN with $SiCl_4$/Ar [2]. The dc self-bias, a negative quantity, was controlled by the rf power (zero rf power ~-10 to -15 V dc bias). The etch rate increased with increasing (negative) dc bias, and was enhanced by a factor of 4 between 150 and 280 V dc bias to yield an etch rate of 660Å at 280 V. A minimum of -100 V dc bias was needed to initiate etching. Another group using $Cl_2/H_2/CH_4$/Ar to etch GaN found that the etch rate increased linearly with increasing rf power [1]. Because the rf power sets the energy of the bombarding ions, both of these results suggest that the sputter-assisted desorption of the etch products is the limiting step.

This rf power dependence is not identical for every type of nitride film. An earlier report by Shul *et. al.* used this same chemistry, $Cl_2/H_2/CH_4$/Ar, to etch GaN, InN and AlN [4]. They reported an increase in etch rate with increasing rf power for GaN as well as InN, providing a maximum etch rate of 2850 Å/min and 3840 Å/min, respectively. The etching began at a setting of 65 W of rf power (or ~-75 V dc bias). These results imply that either the etch products are not desorbed efficiently at low ion energies or that a thin surface oxide is present which must be sputtered away before chemical etching can occur. The AlN etch rate remained essentially constant (with a slight maximum of 1245 Å/min) throughout the range of rf powers applied (including rf power = 0 W), which implies that the either the surface oxide is removed at a low dc bias or desorption of the etch products is more efficient than for GaN or InN. The effect of the removal of Cl_2 from the plasma was noted in another paper, which reported that although the etching rates were much lower than the other chemistry, and were in the range of 280 Å/min (AlN) to ~400 Å/min (GaN) at -250 V dc bias, the etch rates were essentially linearly dependent on dc self-bias over a wide range, reaffirming that desorption of the etch products by sputtering is a key step [1].

A recent investigation by Vartuli *et al.* used ICl/Ar as the plasma to etch GaN, InN, InGaN, InAlN, and AlN [3]. The rf power was ranged from 50 to 250 W. The etching rates of AlN and InAlN were affected very little by the increasing rf power (corroborating the earlier findings for AlN etching using $Cl_2/H_2/CH_4/Ar$), but GaN, InN and InGaN all displayed large increases in etch rate over the same range. This lead to maximum etch rates for GaN, InN and InGaN of 13,000 Å/min, 11,500 Å/min and 7,000 Å /min, respectively. The increase in etch rate for these materials with increasing rf power follows earlier assumptions, and therefore, could be due to the bombarding ions having enough energy to remove the less volatile etch product. This allows the etch to proceed with both I- and Cl- etch products.

VI.2.2. Process pressure

The process pressure dependence of the etch rate is strongly influenced by the other settings of the ECR chamber. The group studying the etching of GaN by $SiCl_4/Ar$ found that, at a microwave power of 300 W, the etching rate increased by an factor of 2 when the pressure was raised from 4 to 10 mTorr [2]. This probably occurs because of the increased contact of the ions from the plasma with the etching surface. If this is the case then the plasma density is a very crucial factor of this mechanism and it is important to note the microwave power, since it has a direct relationship to the plasma density. This clarification will help to interpret the comparison of these results to the results of Shur *et. al.*, who used $Cl_2/H_2/CH_4/Ar$ to etch GaN, InN and AlN. In those findings the etch rate, as a function of pressure, reached a maximum at 2 mTorr and then decreased as the pressure was raised to 10 mTorr. This was at a fixed microwave power of 850 W, which was much higher than the microwave power of the previous experiment. It follows that this experiment was run at a much higher plasma density and the difference in reaction to the increasing pressure can be attributed to that. The rf power was held constant (150 W) during this test, which resulted in an increase in dc bias as the pressure was increased. Higher dc biases are attributed to increased collisional recombination which decreases the plasma density at higher pressures. This decrease in etch rates with increasing pressure and dc biases imply that group III-nitride etching is strongly dependent on plasma density.

VI.2.3. Microwave power

In this same analysis by Shur *et. al.* on $Cl_2/H_2/CH_4/Ar$ etching of GaN, InN and AlN, the effects of microwave power on the etch rate were also investigated [4]. As the microwave power

was increased from 125 to 850 W, the GaN and AlN etch rates increased less that a factor of 2, whereas the InN etch rates increased by more than a factor of 3.5. Increasing microwave power corresponds to an increased ion density, so this trend agrees with the decline in etch rates observed at higher pressures and lower ion densities.

A more recent report on the etching of these same three binary nitride films by HI/H_2 led to similar results [1]. As the microwave power (ion current density) was increased, the etch rates all increased reaching a maximum of ~1075 Å/min, ~1000 Å/min and ~1200 Å/min for GaN, InN and AlN, respectively, at 1000 W. There was no selectivity among the nitrides. Another experiment with similar initial settings, but employing a HBr/H_2 plasma, found that the etch rate (as functions of microwave power) of GaN was close to that of HI/H_2 (~900 Å/min maximum), while the etch rates of AlN and InN were lower (~600 Å/min and 200 Å/min, respectively) [1].

VI.2.4. Electrode temperature

Shul *et. al.* investigated the dependence of InN, GaN and AlN etch rates on the electrode temperature in a $Cl_2/H_2/CH_4/Ar$ plasma [5]. The etch rate of GaN was constant as the electrode temperature was raised from 30 to 125 °C and then increased rapidly to reach a maximum of 2340 Å/min at 170 °C. In contrast, the etch rate of InN decreased from 30 to 150 °C then rapidly increased to reach 2300 Å/min at 170 °C. The AlN etch rate decreased throughout the temperature range studied with a maximum of 960 Å/min at 30 °C. For GaN and InN the increase in the etch rate at high temperatures may be attributed to either an increase in the volatility of one of the etch products or a transition in the dominant reaction mechanism. The initial InN etch rate decrease may be due to competitive reactions between Cl_2 and CH_4 with InN to form either $InCl_x$ or $In(CH_x)_y$, and as the temperature increases above 150 °C, either the volatility of one of the etch products increases or the reaction kinetics becomes dominated by the surface reaction mechanisms. After removing the CH_4 from the plasma, the results were similar, but with slightly lower etch rates. The maximum etch rates for GaN and InN were ~2000 Å/min and ~1500 Å/min, respectively, at an electrode temperature of 170 °C.

VI.2.5. Material quality

The material quality played a part in the work utilizing $SiCl_4/Ar$ plasma as an etchant for GaN [2] The variation in etch rate was observed as a function of material quality, with a smaller rocking curve half-width being indicative of high crystalline quality. The etch rate increase with

respect to a decrease in the material quality gives relevancy to a popular opinion about the significance of high FWHM and high defect densities for higher etch rates. In fact, the etch rate at a FWHM of 260 was only 30% of the rate for a FWHM of 650.

VI.2.6. Percent etchant in the discharge

Without a doubt, the effect of the percentage of etchant in the plasma discharge is greatly dependent on the chemistry of the plasma and the material being etched. Vartuli *et. al.* investigated this effect while etching GaN, InN, InGaN, InAlN and AlN with ICl/Ar plasma [3]. In their results AlN, InGaN and InAlN showed little dependence of the etch rate on % ICl discharge. The InAlN and AlN were not greatly affected by the changes in the composition of the plasma, perhaps because both Al-containing etch products ($AlCl_3$ and AlI_3) have similar volatility. The other two binary compounds, GaN and InN showed an increase in etch rate with ICl addition. It was surmised that there may be a competition between the formation of $GaCl_3$ and GaI_3 (mono and dichlorides are generally only important at high temperature). Another study of this effect was undertaken involving the etching of GaN with $SiCl_4$/Ar plasma [2]. Enhanced rates of etching were obtained as the fraction of active chemical etching species ($SiCl_4$) was increased (with a constant Ar flow rate of 15 sccm), but at $SiCl_4$ >.5 the etched surfaces became rougher. The Ar therefore is believed to insure a smooth etch by efficiently removing the reaction products. A maximum etch rate of 960 Å/min was reported for a pure $SiCl_4$ plasma etch.

VI.2.7. Chemistry of the plasma

The results of etching GaN, InN, InGaN, InAlN, and AlN using a 4 sccm ICl / 4 sccm Ar plasma demonstrate the important role that the chemistry of the plasma plays [3]. Although, the N_2 etch product for the nitrides is still unidentified, the conclusion of this work seems to be that the etch rate changes, with respect to rf power and plasma composition, appear to be directly influenced by the volatility of the group III iodide and chloride etch products. It follows that the choice of ICl as the reactive agent of the plasma directly influences the etch rate.

Zhang *et. al.* were prompted to study the effects of ECR etching of GaN with $SiCl_4$/Ar because ECR leaves less damage than CAIBE, is more uniform than MIE, and this particular chemistry does not does not allow the incorporation of hydrogen [2]. Hydrogen passivation of the III-nitride film is a downfall of using H_2 in the plasma chemistry. By choosing a chemistry without this component such as ICl and $SiCl_4$, this problem is circumvented.

$Cl_2/H_2/CH_4/Ar$ has been a very popular chemistry among researchers [1,4,5]. This chemistry is so commonly used because Cl_2 and CH_4 are responsible for highly volatile group III-chloride and group III-methyl etch products, which improve the etching rates for the III-nitride films. The plasma chemistry, $Cl_2/H_2/Ar$, was also investigated for GaN and InN [5]. The results were very similar to the previous chemistry, $Cl_2/H_2/CH_4/Ar$, but with slightly lower etch rates and less dramatic changes with temperature. The higher GaN and InN etch rates with the presence of CH_4 in the plasma, regardless of temperature, may be attributed to the additional formation of the group III-methyl etch product (which appears to be more volatile than the group III-chlorides below ~150 °C) or an etch mechanism that is enhanced by the CH_4.

The etching of GaN, InN and AlN with HI/H_2 has given results which are a good platform for comparison to similar chemistries. The etch products were assumed to be NH_3 and group III nitrides, and no etch selectivity was seen among the nitrides [1]. In this report, HBr/H_2 was also tested as the plasma chemistry, with the same settings and flow rates as HI/H_2, and the results were consistent with the expected volatilities of group III bromides relative to their iodide counterparts. The etching rates for GaN were fairly close to those using HI/H_2, but the rates for InN and AlN were significantly lower. Therefore a differential undercut can be observed between GaN and AlN or InN materials when HBr/H_2 is used as the plasma chemistry.

The investigation of $CH_4/H_2/Ar$ as the plasma chemistry demonstrated significantly lower etch rates ranging from 280 Å/min for AlN to 400 Å/min for GaN at 1000 W microwave power [1]. This supports the assumption that the presence of Cl_2 enables the formation of highly volatile Cl-containing etch products.

VI.3. Physical effects of dry-etching

Even though the nitrides are more resistant to damage introduction than other III-V semiconductors, the effects of the ion-bombardment and chemical reaction of the plasma with the surface of the III-nitride surface can be significant for certain etch chemistries and ion energies. The damage incurred could be structural or electrical in nature.

VI.3.1 Structural Damage

In a recent experiment, the sidewall profile of a GaN mesa was found to not be vertical due to the apparent recession of the Ni mask used for the pattern transfer [2]. Different masks are chosen depending on such factors as temperature of the electrode and chemistry of the plasma.

Some masks commonly used are: Si_3N_4, $SiN_{0.44}$, Ni or photoresist (AZ 5209E or AZ4330). The sidewall of the laser usually has vertical striations that result from the transfer of roughness of the mask edge onto the semiconductors. During the investigation of using the $Cl_2/H_2/CH_4/Ar$ plasma chemistry for etching, it was hypothesized that the high anisotropy of the etch may be attributed to the possible formation of a sidewall polymer involving the methane [4]. The ability to form very delicate structures is important for device development, and one benefit of the low process pressures employed under ECR conditions is that there is little differential etching between the foot of a mesa and areas out on the field [1]. It was also noticed that the etch rates were significantly higher with improved anisotropy due to the increased ion bombardment energy (rf power). However, high ion bombardment energy also contributes to increased surface roughness, probably due to micromasking from redeposition of sputtered materials or preferential etching of the group III-nitride film. The morphology of the etched surface is equally as important as the anisotropy. The tests of the HI/H_2 plasma chemistry showed that the etched field had similar morphology to unetched mesas, the anisotropy of the etch was very good (leaving a ~75° sidewall angle), and the striations on the side wall are due to the original mask [1]. An example of the relationship between the ion bombardment energy and the surface roughness was demonstrated in a report on the etching of GaN by $Cl_2/H_2/CH_4/Ar$. At rf power values up to ~150 W, the roughness of the etched surface matched the unetched surface roughness, but at rf powers greater than 150 (up to 300 W), the roughness of the etched surface increased rapidly.

Surface roughness is often caused by preferential loss of group V element (N) from the surface due to its higher volatility. Preferential sputtering of N occurs for higher energies, leading to rough GaN surfaces at rf power above ~200 W. In some experiments, such as the ICl/Ar etching tests, the etched surfaces were found to be significantly smoother than that of the as-grown sample indicating that the etch products were removed predominantly by ion assistance [3]. This is also an indication that the morphology of the samples used in this experiment were pretty bad compared to CQD standards, so we should not expect the same etch rates for these chemistries on our material. The differences among the nitride films themselves also contribute to the roughness that one can expect after dry-etching is performed on them. For example, Shul et al. showed that when etching with $Cl_2/H_2/CH_4/Ar$ the smoothness of etched InN surface is more sensitive to rf power, microwave power and process pressure than GaN and AlN [4].

VI.3.2. Electrical damage

A paper by Pearton et al. investigated the electrical damage to the films after dry etching [6]. It was concluded that the combination of high microwave and rf powers produces large increases (10-10^4 times) in sheet resistance of the nitrides, but conditions more typical of real etching processes (rf power <150 W) do not change the electrical properties. The thermal stability of the plasma induced damage was also investigated. The recovery of initial conductivity for InN and InGaN starts at anneal temperatures of ~500 °C and is complete by 650 °C. Assuming that the recovery mechanism was the annealing of the deep acceptor states by diffusion, they estimated an activation energy at around 2.74 eV from the equation:

$$\frac{R}{R_O} = 1 - \exp[-t\nu \exp(-E_d / kT)]$$

where t is time (60 sec), n is the attempt frequency (~10^{14} s^{-1}), T is the absolute anneal temperature and R/R_0 is the ratio of resistances. The 2.74 eV is from a recovery over a broad range of temperatures and, therefore, represents the average of several deep level states with slightly different activation energies. Another paper on dry etch damage by Molnar et al. tested many different plasma chemistries and noted that only etching in $CH_4/H_2/Ar$, CH_4/H_2 and H_2 leads to an increase in the GaN layer's sheet carrier concentration and a decrease in the effective Hall mobility [7]. This effect was not seen after etching in the BCl_3 and Cl_2 plasmas, insinuating that the observed damage is due to the influence of hydrogen on the defect generation. The damage was removed by subsequent annealing of the affected GaN layers at 800 °C. It is believed that chemical, not physical, changes are responsible for this observation. It is now well understood that hydrogen can permeate GaN up to 1 mm and that it acts to passivate shallow donors or acceptors in III-V semiconductors. The annealing reverses the passivation, presumably, by breaking the hydrogen-dopant bond.

Besides physical, chemical and electrical effects, another important requirement is that GaN etch rates should be reasonably fast (>a few thousand Å/min) since the total etch depth is going to have to be on the order of mm. It has been postulated that a recipe with H_2, such as $Cl_2/H_2/Ar$, is best suited for laser fabrication since hydrogen compensation is of less concern, and the etching is faster with the H_2 component.

VI.4. References

[1] C.B. Vartuli, S.J. Pearton, C.R. Abernathy, R.J. Shul, A.J. Howard, S.P. Kilcoyne, J.E. Parmeter and M. Hagerott-Crawford, "High density plasma etching of III-V nitrides" J. Vac. Sci. Tech. A **14**, 1011 (1996).

[2] L. Zhang, J. Ramer, J. Brown, K. Zheng, L.F. Lester and S.D. Hersee, "Electron cyclotron resonance etching characteristics of GaN in $SiCl_4$/Ar" Appl. Phys. Lett. **68**, 367 (1996).

[3] C.B. Vartuli, S.J. Pearton, J.W. Lee, J. Hong, J.D. MacKenzie, C.R. Abernathy and R.J. Shul, "ICl/Ar electron cyclotron resonance plasma etching of III-V nitrides" Appl. Phys. Lett. **69**, 1426 (1996).

[4] R.J. Shul, A.J. Howard, S.J. Pearton, C.R. Abernathy, C.B. Vartuli, P.A. Barnes and M.J. Bozack, "High rate cyclotron resonance etching of GaN, InN and AlN" J. Vac. Sci. Technol. B **13**, 2016 (1995).

[5] R.J. Shul, S.P. Kilcoyne, M. Hagerott-Crawford, J.E. Parmeter, C.B. Vartuli, C.R. Abernathy and S.J. Pearton, "High temperature electron cyclotron resonance etching of GaN, InN and AlN" Appl. Phys. Lett. **66**, 1761 (1995).

[6] S.J. Pearton, J.W. Lee, J.D. MacKenzie, C. R. Abernathy and R.J. Shul, "Dry etch damage in InN, InGaN and InAlN" Appl. Phys. Lett. **67**, 2329 (1995).

[7] B. Molnar, C.R. Eddy, Jr. and K. Doverspike, "The influence of CH_4/H_2/ Ar plasma etching on the conductivity of n-type gallium nitride" J. Appl. Phys. **78**, 6132 (1995).

VII. FABRICATION AND CHARACTERIZATION OF GaN p-i-n MESA STRUCTURES

VII.1. Dry etching of III-Nitrides

Upon the installation of the PlasmaTherm 770 ECR Dry Etching System in January, we began to test the capabilties of a few standard nitride etching chemistries, reported in the literature and summarized in Section VI, on our typical GaN samples. We did not, however, exactly duplicate the recipes and chamber parameters of previous experiments due to differences in our system compared to others. The speed of the etch rate was not our fundamental concern, but rather the quality, controllability and repeatability of the etch itself, and therefore we adapted the previoulsly published recipes to fit our processing needs.

$H_2/Cl_2/Ar$ was the first chemistry tested. Depending on various chamber parameters (e.g. chamber pressure, electrode temperature, flow rates, rf and microwave powers), this chemistry yielded etch rates ranging from 150 to 400 Å/min as measured by scanning electron microscopy (SEM) and step profiler. These etch rates were slightly lower than previously published results due to the lower temperature of our electrode, and, more importantly, the better morphology of our samples. The relationship between film morphology and etch rate is very defined, and logically the closer to ideal single crystal the film is the slower it will etch.

The second chemistry tested was $H_2/Cl_2/CH_4/Ar$, which was similar to the first one with the addition of methane (CH_4). Unlike the other gases which were introduced into the plasma generator above the sample, methane was introduced into the chamber below the sample. Its addition dramatically increased the volatility of the chemistry, leading to etch rates of as high as 3600 Å/min for GaN. These rates were higher than comparable published studies but, again, the differences could be caused by parameters in the chamber such as different magnet settings.

A third chemistry tested was $SiCl_4/Ar$. This chemistry was the one we kept for device fabrication and for etching optimization. It is expected to be better than the others because it does not involve a hydrogen component. Consequently, it is expected to enable us to etch without the risk of passivating the activated p-type layers. The initial runs with this chemistry led to an extrordinarily high etch rate of 7070 Å/min, which was much higher than practical values. By lowering the rf DC bias to -200 V and the microwave power to 300 W, we succeeded in lowering the etch rate to a more practical 1500 Å/min. The etch rate varies slightly for different $Al_xGa_{1-x}N$ alloy composition as well as for different doping (n and p) levels and layer morphology, but we

have generally found it to be consistently between 1500 and 2000 Å/min for a -200 V rf DC bias and 300 W microwave power. These etches were much faster than a previous group found, which is largely due to the elevated temperature of the electrode in our etches used in order to attain a more repeatable process.

We have also tuned the etching parameters (rf and microwave powers) toward specific functions. The rf power, or rf DC bias, controls the energy of the plasma and indirectly the bombardment of the ions (anisotropic etch), while the microwave power controls the density of the plasma (isotropic etch). By decreasing the rf power and increasing the microwave power, we attained smoother and faster etches with practically no electrical and physical damage to the film. Alternately, when we increased the rf power and decreased the microwave power, a more anisotropic etch was achieved with more vertical sidewalls.

The masks reported in the literature are either a photoresist pattern or a Si_3N_4 layer. In our case, we have been using photoresist because it is quick, easy to apply and reliable for accurate pattern tranfer. Moreover, photoresist is not damaged by the plasma etch during the short etches we have been conducting. Any observed roughness in the transferred pattern was mainly due to the initial photoresist pattern rather than to any degradation of the photoresist layer in the etching plasma.. Finally, we also tested the use of SiO_2 as the masking material rather than photoresist. Preliminary results showed that it works as well as photoresist for the patterning effects.

VII.2. GaN p-i-n photodiodes

After our initial tests using the etching system, mesa structures of GaN p-i-n mesa structures for photodiode applications have been fabricated (Figure 2).

These photodiodes consisted of 400 μm x 400 μm mesas. Because the detection areas were much smaller than for our previous devices, the detector response speed was substantially improved, Figure 3. In our preliminary tests, the response speed of these photodiodes was limited by the RC time constant of the measurement circuitry.

The photodiodes also exhibited good responsivity and low noise at zero bias. The peak responsivity was more than three orders of magnitude higher than at wavelengths longer than 400 nm, Figure 4. The response at longer wavelengths was actually limited by the noise of the measurement setup. We are currently trying to improve our measurement setup to reduce noise.

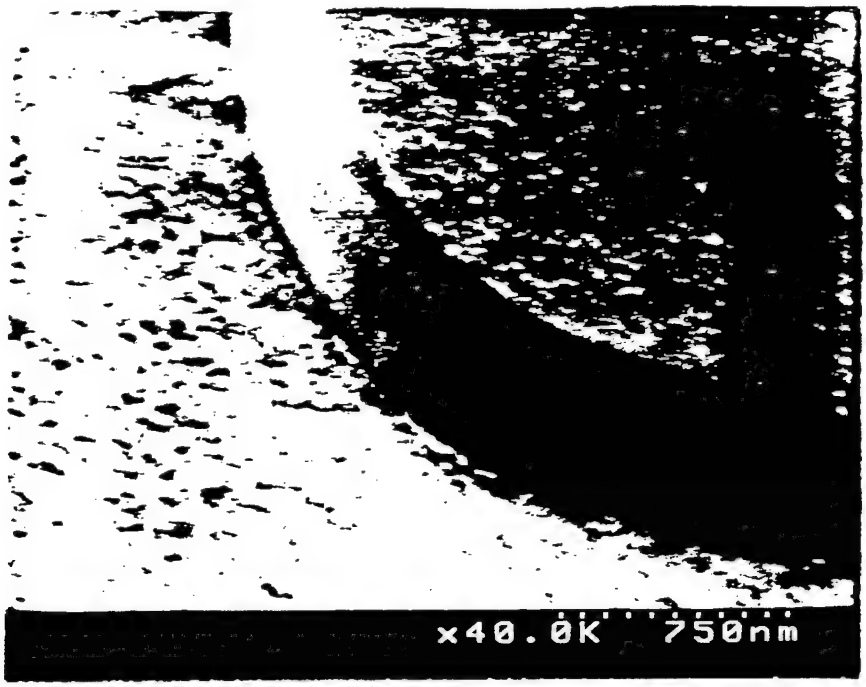

Figure 1. Scanning electron micrograph of the sidewall of a GaN p-i-n structure.

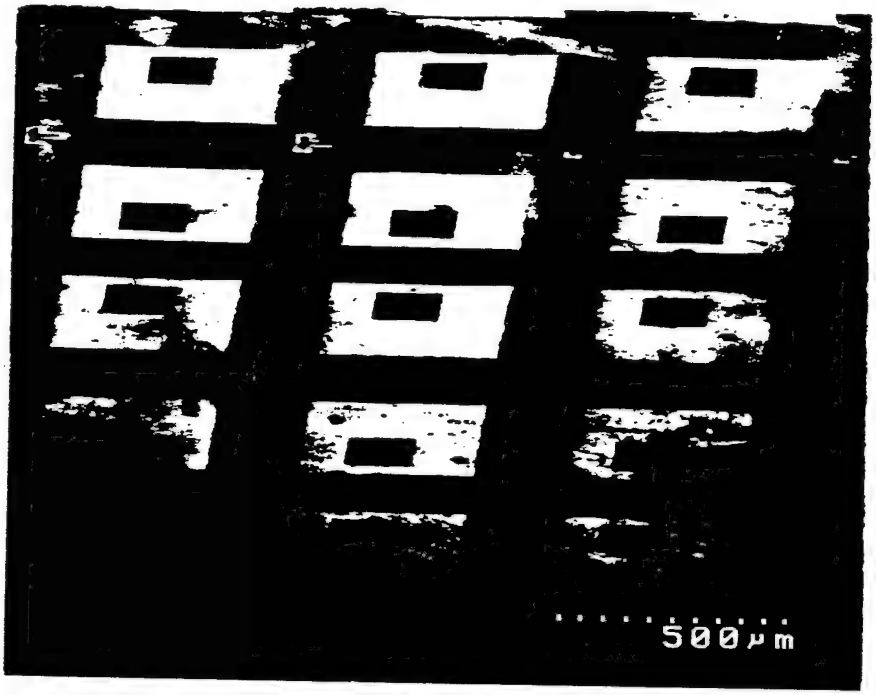

Figure 2. Scanning electron micrograph of GaN p-i-n mesa structures.

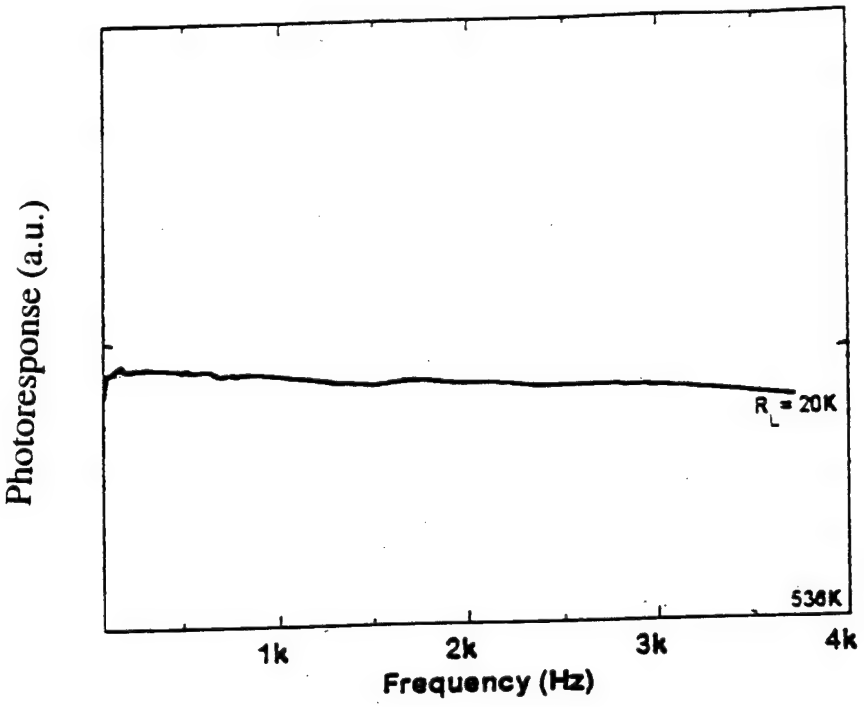

Figure 3. GaN p-i-n photodiode frequency response. The detector speed was limited by the RC time constant of the measurement circuit.

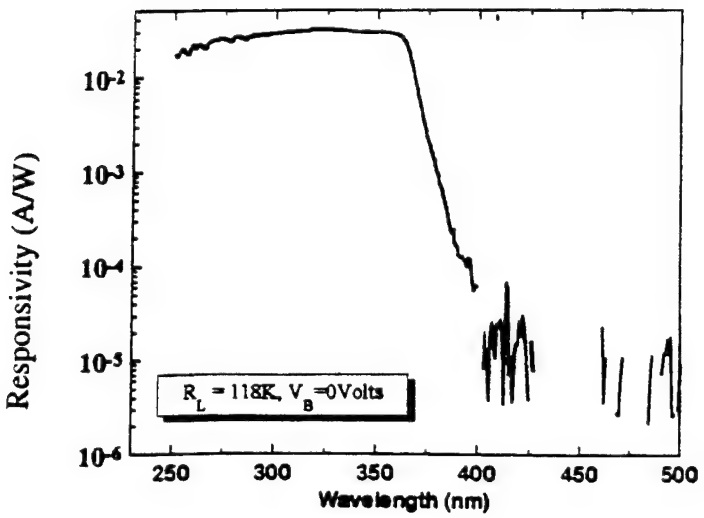

Figure 4. Spectral photoresponse of a p-i-n GaN photodiode at 300K.

VIII. CONCLUSION / FUTURE WORK

In conclusion:

(i) We have conducted the reciprocal space mapping of both symmetric and asymmetric reflections of GaN thin films grown on sapphire substrates. These showed that the primary cause for broadening of the epitaxial GaN x-ray rocking curves was a limited in-plane coherence length. This is consistent with TEM studies which showed threading dislocations originating at the interface, presumably during the initial stages of growth and island coalescence. These dislocations disrupt the coherence length, resulting in broadening of the x-ray rocking curves.

(ii) We have demonstrated a methodology to reduce the density of screw and mixed **dislocation densities** in GaN epilayers on sapphire substrates to **less than ~10^7 cm^{-2}**, as measured by cross-sectional transmission electron microscopy. The structure employed consisted of a GaN/$Al_xGa_{1-x}N$/GaN heterostructure. The dislocations were annihilated at each successive GaN-AlGaN interface, leaving less than 10^7 cm^{-2} in the top GaN layer.

(iii) GaN thin films with mirror-like surface morphologies, good uniformity, narrow X-ray diffraction and narrow bandedge photoluminescence have been obtained **at the same time on the same wafer, with wafer sizes up to two inches in diameter**. Both the n-type and p-type doping of GaN films have been improved.

(iv) The quality of undoped, n-type and p-type doped $Al_xGa_{1-x}N$ thin films on sapphire substrates has been improved for the entire compositional range. The linewidths of the 00•2 X-ray diffraction peaks were lower than 4 arcmins for the whole alloy compositional range. The n-type doping of $Al_xGa_{1-x}N$ was achieved by using Si as the dopant up to an **Al concentration of 50%**. Electron mobilities were higher than 80 cm^2/Vs. The p-type doping of $Al_xGa_{1-x}N$ was achieved by using Mg from GaN up to an **Al concentration of 30%**. We have successfully demonstrated $Al_xGa_{1-x}N$-based Bragg reflectors with controlled peak reflectivity wavelengths, two dimensional electron gas structures, $Al_xGa_{1-x}N$/GaN heterostructures and superlattices exhibiting clear satellite peaks in the X-ray diffraction spectra. These confirm the **quality of the interfaces** in these structures, which is consistent with the **atomic sharpness** observed by cross-sectional transmission electron microscopy.

(v) We have reported **the successful growth of single crystal GaN thin films on β-$LiGaO_2$** by metalorganic chemical vapor deposition. X-ray diffraction linewidths of about 300

arcsecs were achieved with near bandedge photoluminescence at 3.44 eV, thus proving the potential of β-$LiGaO_2$ as a substrate material for the quasi-lattice matched epitaxy of GaN thin films.

(vi) We have demonstrated $Al_xGa_{1-x}N$ based UV photoconductors with tailored cut-off wavelengths from 365 to 200 nm by tuning the alloy composition from GaN to AlN, thus successfully demonstrating the potential of $Al_xGa_{1-x}N$ for ultraviolet photodetector applications. **Detectivity measurements** have been performed and a D* of ~10^9 cm·$Hz^{1/2}$/W was measured at 14 Hz for GaN.

(vii) We have conducted a survey of the state-of-the-art of dry etching of III-V nitrides reported in the literature, which helped us ramp-up our dry etching capabilities.

(viii) GaN p-i-n mesa structures have been fabricated using the newly installed PlasmaTherm 770 Dry Etching System at the Center for Quantum Devices. The **response speed of these p-i-n photodiodes has been significantly increased** in comparison to our previous devices. The speed is now limited by the RC time constant of the detection circuitry.

Future research work on III-Nitrides will be conducted in the following areas:

(i) *Material quality improvement.* Further improvement in the optical and electrical properties of undoped, n-type and p-type doped $Al_xGa_{1-x}N$ thin films will be investigated, in particular for alloys with high Al concentrations because these materials would then be used as barrier layers providing better improved confinement. Higher p-type doping, leading to lower resistivities, for high Al concentration $Al_xGa_{1-x}N$ will be an important focal point.

Moreover, in an on-going effort to further reduce the density of defects in III-Nitride thin films, we will continue to investigate the potential of novel substrate materials, such as SiC and β-$LiGaO_2$ which have a closer lattice match to III-Nitrides than sapphire, for the MOCVD growth of III-Nitrides.

(ii) *Device fabrication and modeling.* Thanks to the new etching capability, prototype device structures will be fabricated and characterized to further probe the III-Nitride material properties. The extracted information, coupled with theoretical modeling, will help improve the design and performance of devices.

IX. List of publications and presentations during 4/96 - 3/97

- "Semiconductor ultraviolet detectors"
  M. Razeghi and A. Rogalski; J. Appl. Phys. **79**, 7433 (1996).

- "Observation of inversion layers at AlN-Si interfaces fabricated by metal organic chemical vapour deposition"
  X. Zhang, D. Walker, A. Saxler, P. Kung, J. Xu, and M. Razeghi; Electronics Letters **32**, 1622 (1996).

- "Metalorganic chemical vapor deposition of monocrystalline GaN thin films on β-$LiGaO_2$ substrates"
  P. Kung, A. Saxler, X. Zhang, D. Walker, R. Lavado, and M. Razeghi; Appl. Phys. Lett. **69**, 2116 (1996).

- "Observation of room temperature surface-emitting stimulated emission from GaN:Ge by optical pumping"
  X. Zhang, P. Kung, A. Saxler, D. Walker, and M. Razeghi; J. Appl. Phys. **80**, 6544 (1996).

- "$Al_xGa_{1-x}N$ ($0 \le x \le 1$) ultraviolet photodetectors grown on sapphire by metalorganic chemical vapor deposition"
  D. Walker, X. Zhang, A. Saxler, P. Kung, J. Xu, and M. Razeghi; Appl. Phys. Lett. **70**, 949 (1997).

- "Development of III-Nitride Technology for Optoelectronic Devices"
  M. Razeghi; DARPA/ETO GaN Workshop, Reston, VA, May 9-10, 1996.

- "MOCVD Growth of High Quality GaN-AlGaN Based Structures on Al_2O_3 Substrates with Dislocation Density less than 10^7 cm^{-2}"

M. Razeghi, P. Kung, X. Zhang, A. Saxler, D. Walker, W. Qian, and V.P. Dravid; International Symposium on Nitrides, St. Malo, France, May 29-31, 1996.

- "Epitaxial Growth of III-nitride Wide Bandgap Semiconductors"
  M. Razeghi; Air Force Wright Laboratory, Wright-Patterson AFB, OH, June 17-18, 1996.

- "Recent Advances in III-Nitride Materials, Characterization an Device Applications"
  M. Razeghi; XII Conference on Solid State Crystals, Materials Science and Applications, Zakopane, Poland, October 7-12, 1996.

- "Development of III-Nitride Technology for Optoelectronic Devices"
  M. Razeghi; DARPA/ETO 1996 Optoelectronics Program Review, Orlando, FL, Oct. 7-10, 1996.

- "Structural and microstructural characterization of GaN thin films and GaN-based heterostructures grown on sapphire substrates"
  M. Razeghi; 8th Seoul International Symposium on the Physics of Semiconductors and Applications (ISPSA-96), Seoul, Korea, Oct. 21-22, 1996.

- "$Al_xGa_{1-x}N$ based materials and heterostructures"
  P. Kung, A. Saxler, X. Zhang, D. Walker, R. Lavado, K.S. Kim, and M. Razeghi
  Mater. Res. Soc. Symp. Proc. **449** (MRS 1996 Fall Meeting).

- "High resolution x-ray diffraction of GaN grown on sapphire subsrates"
  A. Saxler, M.A. Capano, W.C. Mitchel, P. Kung, X. Zhang, D. Walker, and M. Razeghi
  Mater. Res. Soc. Symp. Proc. **449** (MRS 1996 Fall Meeting).

- "Intrinsic $Al_xGa_{1-x}N$ photodetectors for the entire compositional range"
  D. Walker, X. Zhang, A. Saxler, P. Kung, J. Xu, and M. Razeghi; Photonics West 1997, San Jose, CA, Feb. 11-14, 1997.